Annual Report for the Ultra-Clean Fischer-Tropsch Fuels Production and Demonstration Project
Agreement Number DE-FC26-01NT41099

Reporting Period: July 20, 2002 to July 20, 2003

Submitted by:
Steve Bergin, Integrated Concepts and Research Corporation

October 17, 2003

Table of Contents

Submitting Organization

Integrated Concepts and Research Corporation
1115 East Whitcomb
Madison Heights, MI 48071

Subcontractors

Syntroleum Corporation
Suite 1100
1350 South Boulder Avenue
Tulsa, OK 74119

Tiax LLC
Acorn Park
Cambridge, MA 02140-2328

Denali National Park
PO Box 87
Denali Park, AK
99755

Washington Metropolitan Area Transit Authority
3433 Pennsy Drive
Landover, MD 20785

University of Alaska-Fairbanks
PO Box 757520
Fairbanks, AK 99775

West Virginia University
Department of Mechanical and Aerospace Engineering
PO Box 6106
Morgantown, WV 26506-6106

Massachusetts Institute of Technology
Building 31, Room 155
77 Massachusetts Avenue
Cambridge, MA 02139

Disclaimer

Abstract

Program Management
ICRC provided overall project organization and budget management for the project. ICRC held meetings with various project participants, including a group meeting with all participants. ICRC presented at the Department of Energy's annual project review meeting.

SFP Construction and Fuel Production
The GTL plant at the Port of Catoosa is near mechanical completion and subsequent start-up. A dedication event was held on October 3, 2003. Attendees included Assistant Secretary of Energy, Carl Michael Smith and U.S. Member of Congress, John Sullivan (R, 1st, OK).

The plant has been constructed to convert pipeline-quality natural gas into synthetic diesel fuel—standard and arctic grade. Natural gas will be converted to synthesis gas, comprising of H_2 and CO, in the auto-thermal reformer. The synthesis gas enters a two-stage Fischer-Tropsch reactor to produce paraffinic hydrocarbons. These varying chain length paraffinic hydrocarbons are then hydroprocessed to produce finished product. The schedule for formal start-up is slated for early November 2003. Both Syntroleum and Marathon Oil will provide operational support for the facility.

Syntroleum has been working with the fuel demonstration participants to construct a distribution plan for the fuel. First shipments should commence in mid to late November.

As potential follow-on projects, the U.S. Department of Defense and the U.S. Department of Transportation have both expressed interest in the basis of design (DoD, small footprint plants) and fuels from the Port of Catoosa Ultra-Clean Fuels project.

Evaluation of SFP Fuels in Current Diesel Engines
Fuel tests on buses at Denali National Park and the Washington Metropolitan Area Transit Authority will take place during the next year.

SFP Fuel Assessment with Advanced Prototype Diesel Engines
ICRC has not yet finalized agreements for this task with the project's no-cost partners.

Impact of SFP Fuel on Engine Performance
Part of the project is the study of how gas-to-liquid fuel formulations may affect engine performance and emission characteristics. The project will complement the fuel production, engine and emission control system testing programs by parallel investigations on what and how key fuel variables affect engine emissions, and in what ways, by illustrating the fundamental relationships. The project aims at exploring advanced engine design changes from potential future engine-fuel systems that will benefit from the new fuels.

Specific tasks in this project include:

(1) Assessment of how gas-to-liquid fuels impact engine performance and emissions, directly and in blends; to evaluate tradeoffs among fuel properties and blending ratios; to evaluate engine modifications in further improving engine emissions; and to determine combustion and emission characteristics.

(2) Explore opportunities of injection strategy control and exhaust-gas-recirculation (EGR) in pushing limits of NOx/particulates reduction using Syntroleum Fischer Tropsch (FT) fuels produced from small footprint plant (SFP). The engine will be modified for various injection control and EGR systems. Since particulates are expected to be substantially lower with the GTL fuel, limits of NOx reduction via EGR and injection variables will be explored using the specific fuels.

(3) Evaluate exhaust after-treatment systems performance and design tradeoffs available using gas-to-liquid fuels. Optimize the fuel/engine/emission-control system.

Concomitant computer models will be developed for data analysis and interpretation and, if future resources become available, fundamental models and experiments to verify the effects of fuel characteristics on diesel processes most critical to effective engine performance and low emissions will also be developed. Advanced models will focus on fuel chemical composition effects.

This first two tasks fall into this reporting period. Except for the fuel blends, major objectives for this reporting period have been accomplished. Due to the small quantity of available FT fuel, a limited test matrix was implemented that excluded fuel blends. We have analyzed the combustion characteristics and in-cylinder emission formation mechanisms. However, only a limited test matrix and preliminary analyses have been performed so far. Therefore, further testing and more detailed analysis are warranted.

A Cummins model year 2002 ISB 300, 5.9 liter, 6-cylinder, turbocharged, heavy-duty direct injection diesel engine, rated at 224 kW (300 hp) at 2500 RPM, was used in the experiments. The engine has an active cooled EGR system with advanced electronic controls and heavily retarded injection timings for emission controls. Steady-state experiments were run at 1682 RPM at two load points: 25% and 53% loads. In addition to NOx and particulate measurements, detailed combustion characteristics from in-cylinder pressures were analyzed using an analytical model. Injection timing swings and EGR rate changes from factory settings were implemented to discern engine operational changes and fuel properties effects. Standard low sulfur No. 2 diesel fuel (400 ppm sulfur) and one barrel of Syntroleum Fischer Tropsch gas-to-liquid fuel were used.

Results show that Fischer-Tropsch (FT) gas-to-liquid diesel can easily be used in a modern diesel engine with little to no modifications. Compared to No. 2 diesel, FT fuel reduces particulate emission substantially (50-75%), a substantial fraction of it from sulfate reduction. Favorable combustion effects for the FT fuel for late injection timings also contributed significant particulate reduction. For the same engine operating at a typical cruising at mid-load condition, FT diesel fuel reduces NOx emissions consistently from 6-13% versus No. 2 diesel fuel. FT fuel's higher cetane number and a shorter ignition delay allow fuel injection to be further retarded for emission control.

Analysis of combustion characteristics of the FT fuel shows that FT fuel burns faster during the latter part of combustion, in back-to-back comparisons with No. 2 diesel, especially when combustion occurs predominantly during the expansion stroke. Therefore, extremely late injection timing retard, at or after TDC, can be employed for drastic NOx reduction in advanced engines. This also improves particulate emissions.

Conventional diesel fuel normally produces more particulate matter as EGR increases. Results show that FT fuel removes the sensitive dependence of PM production on EGR rate, allowing significant NOx reductions through the use of higher EGR rates before PM levels become substantially large.

FT fuel gives greater freedom to engine designers when trying to optimize engine parameters in modern engines since it provides another set of variables that affect the combustion and emission processes.

A significant amount of work remains to cover a wider test matrix when more FT fuel becomes available. During next year, we plan to perform experiments and analyses aiming at more detailed characterization of both the engine control parameters, such as EGR, and injection timing, together with fuel variables, such as ignition, combustion, and other chemical and physical fuel properties. An expanded experimental design and additional modeling will buttress the initial findings and shed more light on the maximum potential of the GTL fuel. The analytical combustion model will also be refined. Task originally proposed but not covered include studying the effects of fuel blends and after-treatment systems. We started investigation on particulate trap experiments last year and will resume when budget period four continues.

Cold Start Testing

ICRC has completed cold start testing of the Syntroleum fuel. The same tests were run with number one and number two diesel fuels. All cold start tests were completed using a Detroit Diesel Model 50 engine. The test results have been compiled and will be included in the final report at the end of the project. The Syntroleum fuel shows excellent cold start properties. Use of the Syntroleum fuel enabled the engine to start at more the ten degrees lower than traditional fuels. This makes the fuel a good candidate for truck fleets operating in very cold areas.

Demonstration of Clean Diesel Fuels in Diesel Electric Generators in Alaska

The primary goal of the Diesel Electric Generator clean fuels demonstration is to assure the potential users of these fuels that no adverse affects are encountered, while significant advantages are gained. The possible adverse effects to be measured include possible increased wear in the fuel delivery system leading to higher maintenance costs, and to difficulties associated with handling the fuel in arctic conditions. The significant advantages include reduced emissions of criteria pollutants, the ability to recover significantly more heat from the combustion exhaust, and the reduced environmental impacts of possible spills. Based on our literature reviews, we expect that the Syntroleum fuel will give excellent performance in our tests.

The experimental plan is based on a 2000 hour demonstration of the Syntroleum fuel operating in a high efficiency diesel electric generator setup similar to those being used in remote Alaskan power systems. Efficiency, emissions, engine wear, injection timing, heat recovery, and fuel handling issues will be monitored during this testing.

A Detroit Diesel Series 50 generator will be used for the clean fuels testing. This generator was selected because it exhibits the high efficiency associated with the new generation electronic injection engines, including the high compression ratios from turbochargers, but is small enough to allow the maximum number of testing hours to be conducted with the fuel provided under the program.

The on site fuel storage issue was of some concern, as it was not clear if double walled tanks or secondary containment was required for a temporary project. Our initial plan was to use the ISO containers as the primary dispensing container, and to build a gravel pit with a liner for secondary containment. However, the Denali National Park service has agreed to lend us a tank they purchased several years ago, with the university agreeing to pay for the transportation and cleaning of the tank (it has been sitting empty for several years, and has accumulated some surface rust and dirt). This tank is now in place, and is ready to receive the clean fuel when delivered.

Another major question was what to do with the electricity generated in the project. Electrical switching equipment to connect the generator to the university grid is more expensive than the generator, and our initial budget did not provide sufficient funds for a sophisticated switch. Also, the environmental testing requires adjusting the load, and this can be most easily accomplished by use of a controllable load bank. Therefore, we have elected to purchase a computer controllable load bank for this work. This item had a lead time of several months, and was ordered in May of 2003, and is currently being shipped to the university.

The experiments will be controlled and the data collected through a data acquisition and control system based on National Instruments Labview hardware and software.

The demonstration will require baseline emissions and efficiency data on conventional diesel fuel, to be conducted prior to the arrival of the clean diesel fuel. It is expected that the injection timing will need to be adjusted to optimize the performance of the clean fuels. Changing the injection timing is controlled by software, and Detroit Diesel has agreed to provide the necessary "maps" and train our researchers in how to load these into the generator.

Demonstration of Clean Diesel Fuels in Fuel Cells

Fuel cells promise clean, reliable, efficient electrical power, but need a source of hydrogen to operate. Production, storage and transportation and storage of hydrogen are problematic as it is a low energy density gas, and both energy and capital are required for compression and storage systems. For this reason, production of hydrogen from

hydrocarbon fuels at the fuel cell site is preferable, especially from easily transportable liquid fuels. However, the reforming of conventional distillate fuels, especially logistical fuels preferred by the military, is problematic for several reasons, including the difficulty in vaporizing the fuels, the presence of sulfur, and the difficulty in reforming aromatic compounds. The clean synthetic fuels are ideal for reforming, having no sulfur, relatively low vaporization points, and the predominance of straight chain hydrocarbons.

This project is to demonstrate a fuel cell operating on the naphtha fraction of the clean fuels. This naphtha fraction is lighter than the synthetic diesel product, and so should vaporize easily, thus enabling the reaction to proceed without the formation of solid carbon (coking). Proof of this may establish a market for the naphtha fraction of the fuels.

Experimental Section

Cold Start Testing

Figure A: NETL Clean Fuel Project
Cold Cell Box / Battery Wiring Layout

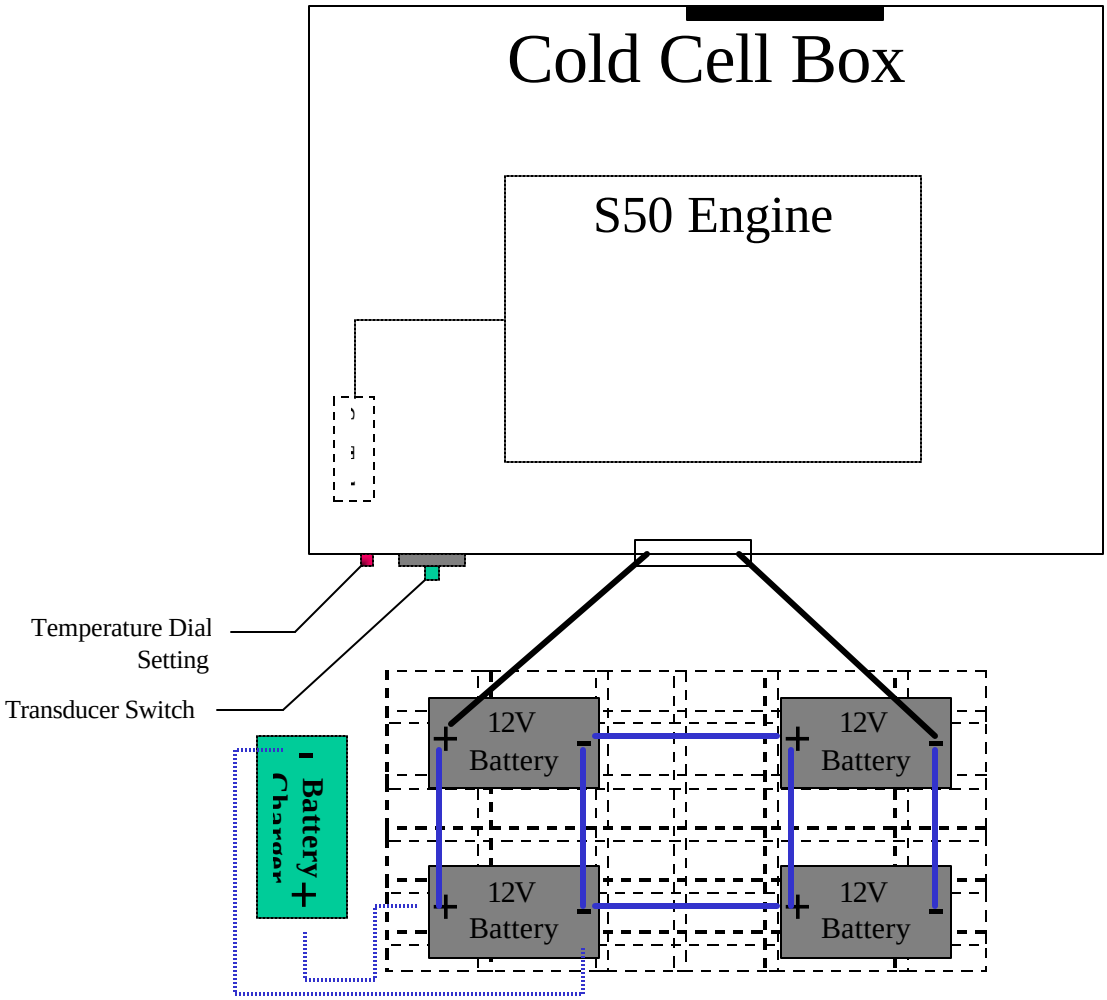

Impact of SFP Fuel on Engine Performance

Cummins supplied a close-to-production development engine based on the model year 2002 (MY02) ISB 300. The ISB 300 is a turbocharged, 6-cylinder, 5.9-liter direct injection diesel engine. The engine is rated at 224 kW (300 hp) at 2500 RPM and 890 N-

m (660 lb-ft) torque at 1600 RPM. In order to meet 2002 EPA standards, the engine has advanced subsystems like a Bosch common-rail fuel injection system, Holset variable geometry turbocharger, and cooled-EGR system. To control these devices, the ISB 300 has an electronic control module (ECM) (version CM 850) that has been calibrated to meet emissions when operating with an EPA No. 2 diesel fuel.

The pre-production ISB 300 engine came equipped with an unlocked ECM, allowing for engine calibration changes and real-time monitoring and modification of engine parameters. To communicate and link to the engine's ECM, Cummins provided their in-house software, CalTerm (Calibration Terminal) version 7.63. Once the engine was installed, the stock 300-horsepower calibration, based on No. 2 diesel and provided by Cummins was uploaded into the ECM. This was done to ensure the engine would run on the 2002 EPA-emission-certified performance maps.

CalTerm allows for the monitoring and modification of hundreds of engine parameters. The important parameters modified in the experiments include the start of main injection and EGR fraction. The response time after commanding an injection timing change is trivial, since the electronic control of fuel injection with the common-rail system provides a response time dependent only upon the speed of the signal from the ECM. For adjustments to the EGR fraction, changes take a few seconds to settle since the ECM tries to find the best path to move to a different state. The coupling of engine load, turbine inlet pressure, turbine exhaust backpressure, intake manifold boost pressure, and EGR valve position required the ECM to optimize changes to prevent the system from reaching an unstable state. One last commanded parameter that was changed enabled cylinder cut out. During engine shakedown and TDC determination (see Section 5.4.1.1), the engine parameter FSI_x_ExtCylMask_c was set to 001F (hexadecimal representation of cylinder 6) in order to cut fueling to the cylinder so that motoring pressure traces could be recorded.

Various other parameters were monitored and logged, including charge flow, pilot injection quantity and timing, post injection quantity and timing, and common-rail accumulator pressure.

Dynamometer Setup and Dynamometer Controller

A Digalog AE 250 eddy current dynamometer, able to absorb up to 250 kW, was used to load the engine. A Maywood Instruments U4000, 500 kg load cell measures torque by resisting the rotation of the outer casing. A differential pressure switch on the cooling-water outlet protects the dynamometer from failing if the cooling water supply happens to shut off.

Connecting the engine to the dynamometer is a driveshaft assembly made with two Spicer 1710 Series flange yokes attached to a 10.16 cm (4") O.D. tube. The flange yokes are rated to withstand up to 1220 N-m at steady state or spikes of up to 6500 N-m. The drive-shaft is installed at about an 8° to relieve stresses in the flange yokes as they rotate.

A Digalog Model 1022A-STD dynamometer controller was used to control engine speed while reading out the load from the Maywood Instruments load cell. The PID settings in the dynamometer controller were also adjusted to reduce load fluctuations when the commanded throttle setting changes. Before any tests were run, the controller and dynamometer were calibrated at two points, the 50% and 100% loads of the engine.

Data Acquisition System

A full complement of National Instruments data acquisition (DAQ) hardware and software was used to measure and record various temperatures, pressures, and flows. The heart of the system is the high-speed DAQ board, a National Instruments PCI-6024E. This board can read up to 200,000 samples per second. The high-speed DAQ board is limited to 16 single-ended channels (signals with a common ground) or 8 differential channels (signals with separate grounds). In order to get around this limitation, an SCXI-1000 multiplexing chassis was also used. The SCXI-1000 chassis can house up to 4 special modules, containing various signal amplification, isolation, and noise suppression circuitry. The multiplexing chassis works by quickly scanning, one after another, all the channels of each module installed streaming the data into one differential channel of the DAQ board.

A special 32-channel module for thermocouples (SCXI-1102B) containing a fixed low-pass filter of 200 Hz was installed into the multiplexing chassis. The SCXI-1102B allows for gain and filter settings to be programmed on a per-channel basis. Most slow-speed signals were connected to this module. Attached to the SCXI-1102B is a TBX-1303 terminal block. The TBX-1303 provides a convenient location for the sensors to wire into while also containing a cold-junction-compensation sensor to provide a reference voltage to correctly scale any thermocouples plugged into the terminal block. A general 32-channel module (SCXI-1100) was used for mixed measurements. This module has user-selectable low-pass filter settings (4 Hz, 10 kHz, and no filter) that apply to all channels. Since high-speed cylinder measurements (see Section 0) were recorded through this module along with various slow-speed signals, the 10 kHz filter setting was used to provide some noise filtering while preventing the possibility of introducing phase errors into the high-speed signals due to poor low-pass filter response. Another TBX-1303 terminal block is attached to the SCXI-1100 module to facilitate sensor wiring.

High Sampling Rate Measurements

High-speed measurements taken during the experiments consisted of in-cylinder pressure, intake manifold pressure, and engine-position-indexing signals. Since in-cylinder pressures in a diesel engine can rise very rapidly after the auto-ignition event, a high-resolution crank-angle encoder was installed onto the tone wheel to act as an external clock to the DAQ system. An 1800-pulse-per-revolution BEI encoder provides a 0.2° resolution for the high-speed data. The BEI encoder also has another channel that gives out one digital pulse per revolution. This once-per-revolution signal was used to trigger the high-speed DAQ measurements, ensuring the data recording started at the same point

of an engine revolution, although not always on the same stroke. This removed the need to superimpose a reference signal to the cylinder pressure data.

The pre-production ISB 300 engine installed at MIT was actually used at Cummins to perform development work on the engine currently available on the market. When the engine was shipped to MIT, an AVL QC33C heavy-duty pressure transducer was already installed in cylinder number 6 (cylinder closest to flywheel). The QC33C is a quartz, piezo-electric pressure transducer that is actively liquid-cooled to reduce the effects of thermal shock. A Bernard Model 2500SS MIG welder cooler is plumbed into the pressure transducer and circulates and cools a 50:50 mixture of distilled water and ethylene glycol. The transducer's small current output is converted to a voltage using a Kistler Model 5010B charge amplifier. The charge amplifier's output is fed into the DAQ system.

Since piezo-electric pressure transducers only measure changes in pressure, a method of referencing the pressure is required. The intake manifold pressures recorded along with the in-cylinder pressure provide a value to peg the cylinder pressure. The in-cylinder pressure signal is usually averaged around BDC and then scaled to equal the intake manifold pressure.

In order to provide precise fueling, the engine's ECM not only must know where the pistons are in relation to TDC, it also needs to differentiate which aspect of the four-stroke cycle each piston is going through. To provide engine-position data, the engine has Hall-effect sensors on both the camshaft and tone wheel. The tone wheel is a 60 (-1) design, originally containing 60 equally spaced teeth with one removed to provide a point of reference. The signal from the tone-wheel sensor was also fed into the DAQ system to check the phasing of the in-cylinder pressure signal.

High Sampling Rate, Crank-Angle Resolved, Data Integrity

The proper phasing of in-cylinder pressure signals is important if further analyses such as IMEP calculations are done with the data. Various checks are available to test for the proper phasing of the data, such as the linearity of the compression and expansion stroke curves in log-P vs. log-V graphs and confirmation that the two curves do not cross each other.

Cummins engineers suggested two ways to correctly phase the start of high-speed data recording with respect to TDC. The first suggestion was to adjust the crank angle encoder such that the reference signal on the tone wheel (the point where the signal goes from high to low after the missing tooth) occurs 60.0° bTDC. Another suggestion was to find the peak pressure during a motoring pressure trace (see Section 5.2 for cylinder cut-out information), then add 0.4° due to heat transfer and blow-by effects. A combination of both techniques was used to check both methods. Initially, the first suggestion was tried, and the crank angle encoder was adjusted such that the high-to-low transition following the gap occurred at 300° as TDC intake was chosen as 0° (see Figure 5.1).

Triggering the crank-angle encoder with this setup resulted in a peak motoring pressure at 361.2° with the addition of heat transfer and blow-by giving an actual engine-TDC of 361.6° (see Figure 5.2). Although the peak pressure occurred 61.2° after the reference signal, this is still within the anticipated uncertainty of the tone-wheel/crankshaft sensor setup.

With the knowledge of the correct phasing of engine-TDC and the crankshaft reference signal, the crank-angle encoder was finally adjusted such that engine-TDC occurred at 360.0°, as everything is referenced with TDC intake as 0.0°. This necessitated encoder adjustments such that the crankshaft reference signal occurs at 298.4°, or 61.6° bTDC (see Figure 5.3). Motoring pressure traces were tested with this final crank-angle encoder setup as a last check for correct phasing.

The test engine and dynamometer is heavily instrumented with various thermocouples and transducers. Tale 5.2 lists the type of sensor, its location in the test setup, and which channel and module it is connected to. The following sections provide further details about special sensors used during the experiments.

Fueling System

To measure fuel flow, two Exact Flow Model EFM84 single-rotor turbine flow meters are used, one measuring fuel supplied to the lift pump that supplies the high-pressure common-rail fuel pump, and the other measuring fuel returning to the fuel tank. Each flow meter has an Exact Flow IFC-14 flow computer calibrated with fuel flow rates versus fuel viscosity. Temperatures from a thermocouple in the flow meter allow the flow computer to correctly read out fuel flow even as fuel temperatures fluctuate. To help keep fuel temperatures steady, a liquid-liquid heat exchange was installed upstream of each fuel flow meter. Exact Flow provided flow computer calibrations for each fuel based on viscosity information from the specification sheets show in Fuel Specifications section. The stock fuel filter on the engine was retained so no filter elements were installed upstream of the flow meters.

In order to prevent cross contamination of sulfur and aromatics between the two fuels used in the experiments, two 81.4-liter (22-gallon) ATL Inc. SP122B racing fuel cells were installed on the engine test bed. Two bulkhead connections near the engine allow switching between the individual fuel tanks. Another bulkhead allows for fuel to bypass the return system in order to drain the entire system or purge standing fuel in various fuel galleries in the engine when changing fuels. The entire fuel system uses Teflon lines since diesel fuel is a strong solvent, while stainless-steel over-braids over the Teflon protect them from physical wear and tear.

Intake Air Measurement and Preparation

An Eldridge Products, Inc. Series 8732 thermal mass flow meter measures airflow into the turbocharger's compressor inlet. The inline-style flow meter consists of a sensing element, installed into a flow section. The flow section has a laminar flow element to

ensure fully developed flow by the time the air reaches the sensing element. The sensing element uses two RTDs (resistance temperature detector) to measure airflow. One RTD measures the temperature of the incoming. The second RTD is forced through self-heating to maintain a constant temperature above the incoming gas. The sensing element's signal processor takes both the required current to heat the second sensor and the initial temperature read by the first RTD to calculate the mass of air flowing through the flow section. A K&N paper filter fitted upstream of the thermal mass flow meter filters the ambient air in the test cell before it flows into the engine.

Table 1 Sensor, sensor location, and module/channel it is wired to.

DAQ Measurement	Instrument Type	Module 1	Module 4	PCI-6024E
Cylinder 1 Exhaust TC	Type K TC	0	N/A	N/A
Cylinder 2 Exhaust TC	Type K TC	1	N/A	N/A
Cylinder 3 Exhaust TC	Type K TC	2	N/A	N/A
Cylinder 4 Exhaust TC	Type K TC	3	N/A	N/A
Cylinder 5 Exhaust TC	Type K TC	4	N/A	N/A
Cylinder 6 Exhaust TC	Type K TC	5	N/A	N/A
EGR TC - Before Cooler	Type K TC	6	N/A	N/A
EGR TC - After Cooler	Type K TC	7	N/A	N/A
Heat Exchanger - City Water Out	Type K TC	8	N/A	N/A
Heat Exchanger - Engine Coolant In	Type K TC	9	N/A	N/A
Turbine Outlet TC	Type K TC	10	N/A	N/A
Intake Manifold TC	Type K TC	11	N/A	N/A
Exhaust Manifold TC	Type K TC	12	N/A	N/A
Coolant Reservoir TC	Type K TC	13	N/A	N/A
Heat Exchanger - Engine Coolant Out	Type K TC	14	N/A	N/A
Heat Exchanger - City Water In	Type K TC	15	N/A	N/A
Engine Block Oil TC	Type K TC	16	N/A	N/A
Compressor Outlet TC	Type K TC	17	N/A	N/A
Fuel Supply TC	Type K TC	18	N/A	N/A
Dynamometer TC - Inner Loss Plate	Type K TC	19	N/A	N/A
Dynamometer TC - Outer Loss Plate	Type K TC	20	N/A	N/A
Dynamometer TC - Bearing #1	Type K TC	21	N/A	N/A
Dynamometer TC - Bearing #2	Type K TC	22	N/A	N/A
Dynamometer Water Pressure	Pressure Transducer	23	N/A	N/A
Exact Flow Fuel Flow Meter - Return	Turbine Flow Meter	24	N/A	N/A
Exact Flow Fuel Flow Meter - Supply	Turbine Flow Meter	25	N/A	N/A
Engine Block Oil Pressure	Pressure Transducer	26	N/A	N/A
Turbine Exhaust Pressure	Pressure Transducer	27	N/A	N/A
Intake Manifold Pressure	Pressure Transducer	28	N/A	N/A
Fuel Lift Pump Pressure	Pressure Transducer	29	N/A	N/A
Exhaust Manifold Pressure	Pressure Transducer	30	N/A	N/A
Coolant Reservoir Pressure	Pressure Transducer	31	N/A	N/A
Cylinder 6 Pressure Transducer	Pressure Transducer	N/A	0	N/A
Fluke Current Probe	Hall-Effect Sensor	N/A	1	N/A
Intake Air Flow	Dual RTD	N/A	2	N/A
Dilution Tunnel - Pre Dilution	Type K TC	N/A	3	N/A
Dilution Tunnel - Post Dilution	Type K TC	N/A	4	N/A
Ambient Temperature	Type K TC	N/A	5	N/A
Post-Filter TC	Type K TC	N/A	6	N/A
Pre-Filter TC	Type K TC	N/A	7	N/A
Engine Torque	Digalog Controller	N/A	10	N/A
Engine RPM	Digalog Controller	N/A	11	N/A
Charge Air Cooler	Type K TC	N/A	13	N/A
Heated Sample Line - Short	Type K TC	N/A	14	N/A
Heated Sample Line - Long	Type K TC	N/A	15	N/A
HFID Range 1 - 8	0 - 5 VDC	N/A	16 - 23	N/A
HFID Voltage	0 - 5 VDC	N/A	25	N/A
HFID Oven Temperature	0 - 5 VDC	N/A	26	N/A
PM Sample Flow Rate	0 - 5 VDC	N/A	29	N/A
NOx Voltage	0 - 10 VDC	N/A	30	N/A
NO Voltage	0 - 10 VDC	N/A	31	N/A
Cummins Crankshaft Sensor	Hall-Effect Sensor	N/A	N/A	2

After being compressed by the turbocharger, the pressurized air leaving the turbocharger is extremely hot. To reduce peak pressures in the engine, the compressed air is cooled once it leaves the compressor. A Spearco Universal Air/Liquid Intercooler was used to cool the fresh charge leaving the turbocharger. The amount of charge-air cooling is controlled by a gate valve on the liquid side of the charge-air cooler that controls the flow of water through the core of the charge-air cooler. Connections between the engine and aftercooler are made with 7.54 cm (3") I.D. silicone rubber hose, capable of withstanding temperatures up to 450 K.

Figure 2: Gaseous Emissions Analyzers

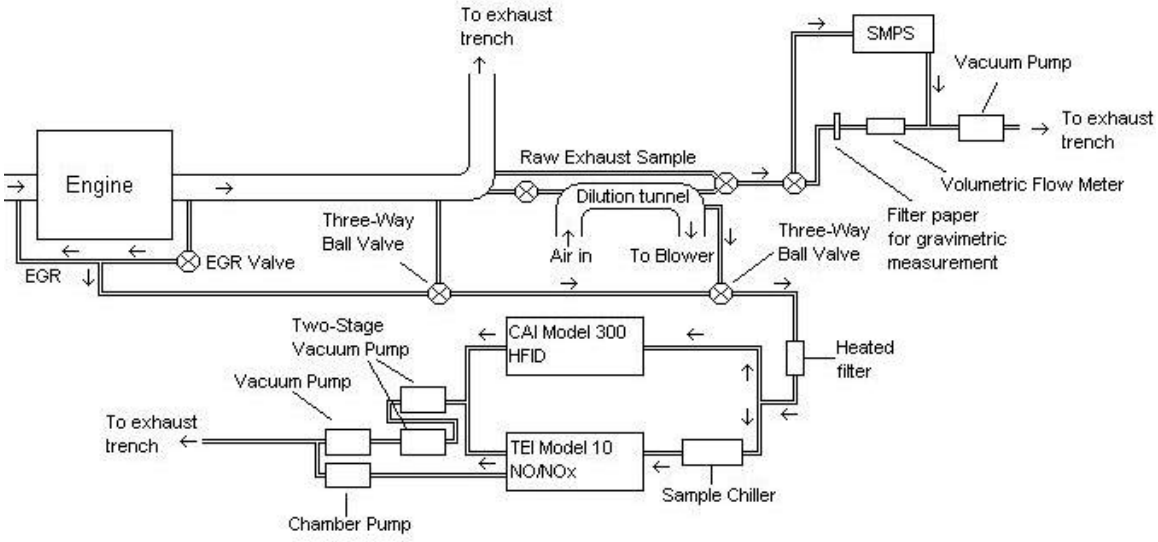

Figure 2 Emission sampling system schematic.

Figure 2 shows a schematic of the emission sampling system. A Thermo Environmental Instruments (TEI) Model 42C-HL (High Level) chemiluminescence analyzer was used to measure the oxides of nitrogen from various sample streams. For engine-out NO_x, a sample point about 0.762 m (30") away from the closest exhaust elbow (1.372 m (54") total distance from turbine exhaust) was installed. This point is about 10 pipe diameters away from the elbow, ensuring fully developed flow at the sample point. For intake-mixture NO_x (for EGR fraction calculations), a sample point 0.1016 m (4") downstream from the closest elbow (0.3048 m (12") from EGR valve) was installed. The intake sample point was installed in the middle of the intake air heater, the heating elements within the flow stream acting as guide vanes, helping to distribute the flow uniformly. For dilution ratio measurements, a sample point was installed about 0.762 m (30") away from the transfer tube, again ensuring fully developed flow at the sampling point. To calibrate the Model 42C-HL, a calibration gas of 998 PPM of NOx and zero gas of pure N_2 was used to create a linear voltage output between the two concentrations. This

output of is fed into the DAQ system, and the voltage read is converted back to a PPM concentration and recorded. For the chemiluminescent reaction, pure oxygen is fed into the meter, converted to ozone, and then used in the reaction chamber. The Model 42C-HL was kept on the 0 – 1000 PPM range for all tests.

The TEI Model 42C-HL uses a Vacuubrand MD4 three stage, four head diaphragm pump to provide the proper vacuum for the reaction chamber. Also, to prevent clogging the capillary tubes inside, a Universal Analyzers Model 530SS single channel sample cooler is used to condense out any water in the exhaust stream. The sample chiller uses a thermoelectric cooler operating on the Peltier effect to bring gas temperatures down to about 4.5° C, removing most of the water that can condense within the temperatures found in most gas analyzers. Thus, all NO_x measurements are on a dry exhaust basis.

To measure hydrocarbon emissions, a California Analytical Instruments (CAI) Model 300-HFID was installed. The Model 300-HFID was calibrated with 300 PPM propane (C_3H_8), so the effective range was 0 – 900 PPM of C_1. During experiments, the Model 300-HFID was left on the 0 – 30 PPM range since HC emissions from diesel engines are low. To measure HC, a flame ionizes the sample stream and electrodes in the instrument measure the particles. The flame in the Model 300-HFID is fueled by HC-free air and a fuel mixture of 40%/60% H_2/He.

The Model 300-HFID takes gas samples from the same points as the Model 42C-HL. All engine and dilution sample points are connected to a bulkhead holding various 3-way valves to switch between various sample points. The engine-out gas stream is transferred to the bulkhead using a 7.62 m (25') heated sample line while the two cooler sample points use stainless-steel-overbraid Teflon tubes. All samples from the bulkhead are moved using a 3.048 m (10') heated sample line to a Universal Analyzers Model 270S heated stack filter that removes any large particulate matter that can also clog sample and capillary tubes within the gas analyzers. To move the gases through all the filters and gas analyzers, two vacuum pumps were used. With the engine-out and intake samples, the gases are above atmospheric pressure, requiring a less-robust vacuum pump to move samples. A Gast Model IVAF-10-M100X rotary-vane vacuum pump was first used in these applications. However, the flow rate with this pump was not sufficient to supply the sample requirements for both gas analyzers. An Air Dimensions Incorporated (ADI) Model 01620TC high-vacuum, double-head diaphragm vacuum pump was installed in series with the Gast pump to increase sample flow rates and reduce the lag time when changing between sample points. The two heads on the ADI vacuum pump were connected in series, effectively giving the system a three-pump arrangement.

Mini Dilution Tunnel

The EPA defines particulate matter as all solid matter and condensable species that can be collected on a paper filter from a diluted exhaust sample held at no higher than 52°C [12]. The EPA defines particulate matter in such a way since it forces the sampling system to employ some form of a dilution tunnel that helps simulate particle transformations (i.e. agglomeration, adsorption, and nucleation) that would normally

occur outside of the laboratory. Dilution tunnels can be designed to condition the entire exhaust flow or can be arranged in such a way as to only take and dilute a small sample of the exhaust.

The mini dilution tunnel used with the experimental setup is based on the dilution of a fraction of the exhaust stream. The dilution tunnel is predominantly made of 75.4 cm (3") O.D. stainless steel 304 tubing. The exhaust gas sample is transferred, due to a positive pressure differential, through a 1.88 cm (¾") O.D. tube with a high-temperature resistant ball valve in place to regulate exhaust gas flow. The transfer tube introduces raw exhaust into the dilution tunnel 0.762 m (30") away from the sample point, allowing the dilution air and raw exhaust to mix and become fully developed before being sampled. The pressure in the dilution tunnel is held below atmospheric conditions by connecting the exit of the dilution tunnel to the intake of a Spencer Model 1001-½SS blower. As air is drawn through the mini dilution tunnel, the pressure drops due to losses within the tubing. A Solberg FS-31P-250 air filter holder with a HEPA filter element is installed at the inlet of the dilution tunnel system, providing an additional pressure drop within the tunnel. The dilution ratio is measured by comparing the NO_x readings in the tunnel to the NO_x readings in the raw exhaust.

Gravimetric Particulate Matter Sampling System

The gravimetric particulate matter sampling system used to sample raw and dilute gas samples employs a Pall Corporation stainless steel 47mm filter holder that housed Pall Corporation Pallflex® Fiberfilm glass filters (Model T60A20-47 MM). Made with borosilicate glass fibers and a moisture-resistant fluorocarbon (TFE) coating, the Pallflex Model T60A20 brand of filters resist moisture uptake and prevent moisture-gas reactions, eliminating the need for lengthy drying times when using normal hygroscopic glass fiber filters. As such, the EPA recommends the Model T60A20 brand of filters for use in gravimetric filter measurements [13]. The Model T60A20 filters can also withstand very high temperatures, up to 315.5°C, making it ideal for raw exhaust gas sampling as well.

To measure sample flow through the filter, an Omega FVL-1611 volumetric flow meter was installed downstream of the filter/filter holder assembly. The Omega FVL-1611 sensor body houses a differential pressure transducers, a thermocouple, and a laminar flow element that the flow computer uses to measure flow rates up to 250 SLPM. The flow computer output is fed into the National Instruments DAQ system, so flow rates over time can be recorded, then averaged. This helps account for the variation in flow rates as the filter paper is loaded. A Millipore Model 6675 piston-driven vacuum pump was used to draw the raw or dilute sample through the sampling lines, filter paper, and mass flow meter. To prevent condensation of particles on the walls with raw exhaust samples, the stainless steel lines from the raw exhaust sample point were insulated with silicon-rubber based tubing insulation. Also, a rope heater was installed from the sample point to a position 1.524 m (5 feet) downstream.

To weigh filtered samples, an Ohaus Explorer E11140 microbalance, accurate to 0.1 mg was used. It was left on for at least one hour to warm up before any filters were weighed.

SMPS System

For a detailed description of the Scanning Mobility Particle Sizer (SMPS) system, see Hallgren [14]. Backgrounds scan with and without the HEPA filter installed upstream of the dilution tunnel is found in Figure 5.6 showing the effectiveness of the HEPA filter. Other than the HEPA filter, no other dilution-air preparation was done.

Due to the short supply of FT fuel available (one 203.5 liter (55-gallon) drum), no runs with the SMPS system were recorded when the data presented in Figure 5.6 was recorded. However, since the test engine has an EGR system, some characterizations of the effects of EGR on PM size distribution were done with No. 2 diesel while the test setup was being shaken down. Please see a subsequent Section for a discussion of these scans.

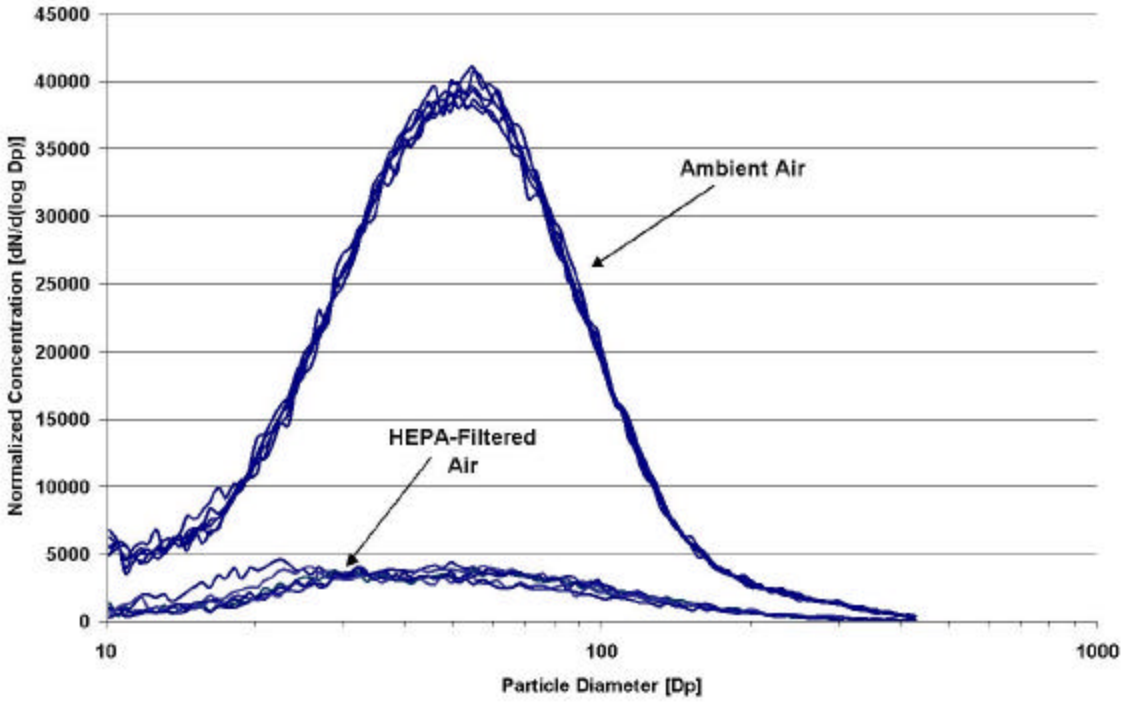

Figure 3 SMPS background scans with and without the HEPA filter installed.

Results and Discussion

Cold Start Testing

ICRC has completed cold start testing of the Syntroleum fuel. The same tests were run with number one and number two diesel fuels. All cold start tests were completed using a Detroit Diesel Model 50 engine. The test results have been compiled and will be included in the final report at the end of the project. The Syntroleum fuel shows excellent cold start properties. Use of the Syntroleum fuel enabled the engine to start at more the ten degrees lower than traditional fuels. This makes the fuel a good candidate for truck fleets operating in very cold areas.

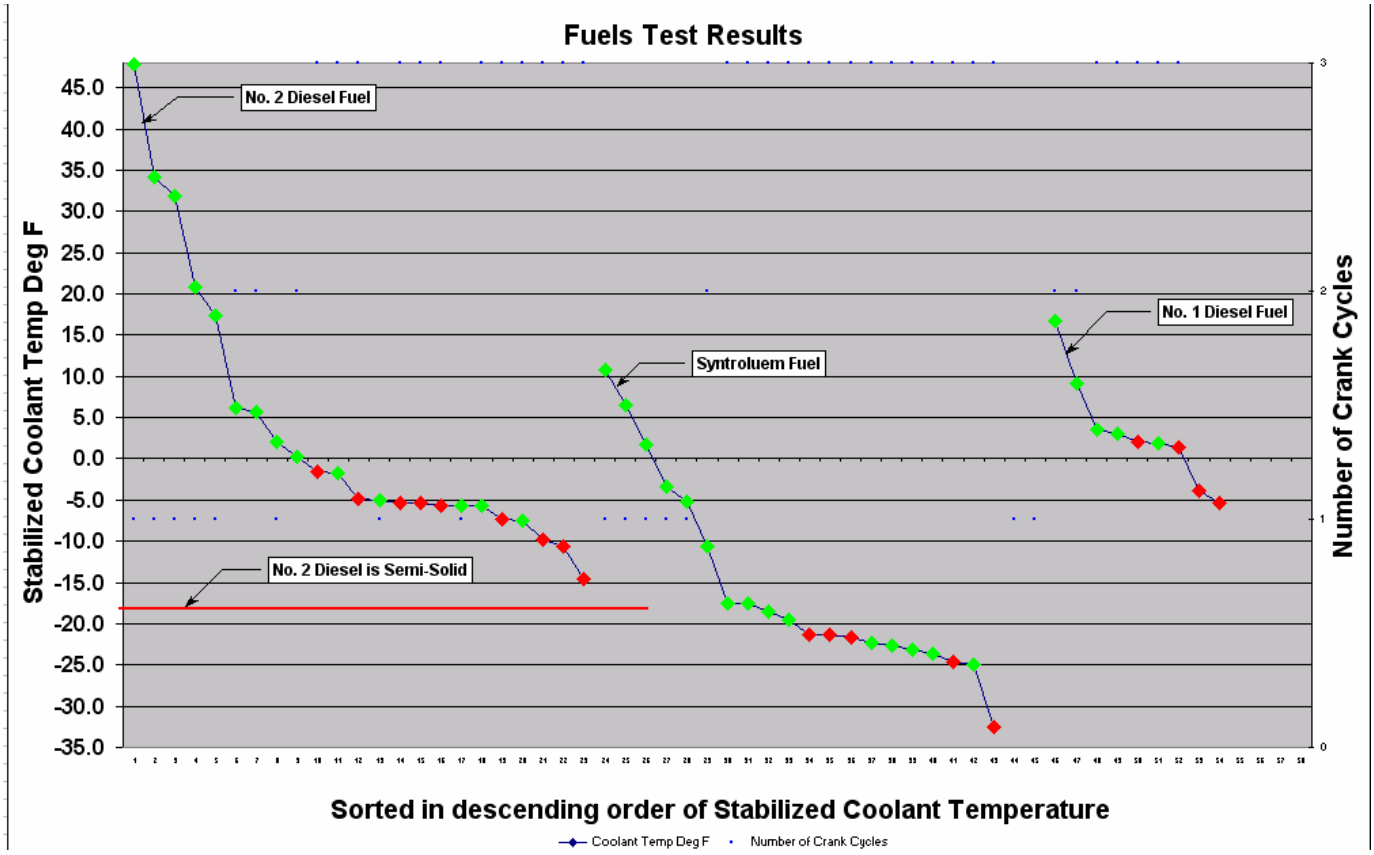

Figure b: Cold Start Testing Results

Impact of SFP Fuel on Engine Performance

Combustion Characteristics

Recently, the combination of various laser-imaging tests [20-27] that tracked various aspects of the reacting fuel jet such as fuel distribution and chemical species such as hydroxyl (OH) radicals and nitrous oxide (NO) spatially and temporally have led to a more complete understanding of the development of the diesel combustion process. The major difference between the old model and the new phenomenological model is that all of the fuel goes through two oxidation stages, first partially oxidizing in a fuel-rich premixed flame and then completing oxidation in a stoichiometric, or very-near stoichiometric diffusion flame. As such, the physical characteristic of the spray is very different from the previously believed model for diesel combustion.

These new revelations of diesel combustion describe the major physical characteristics and processes of combustion such as the spatial and temporal development of the fuel-air plume, equivalence ratios of the standing premixed flame and surrounding diffusion flame, and spatial regions where emissions are most likely forming. Many other details about the combustion event are also important when trying to gain a fundamental understanding of the effects of fuel properties on engine performance and emissions. Interpretation of our current results in light of the new understanding of combustion was performed. Additional analyses with the heat-release-rate curves give such details as how soon after injection the initial premixed burn fraction occurs, crank-angle locations of when certain percentages of the total energy is released, or when the end of combustion occurs. These and other parameters are helpful in determining why fuel properties affect an engine's overall operating characteristics.

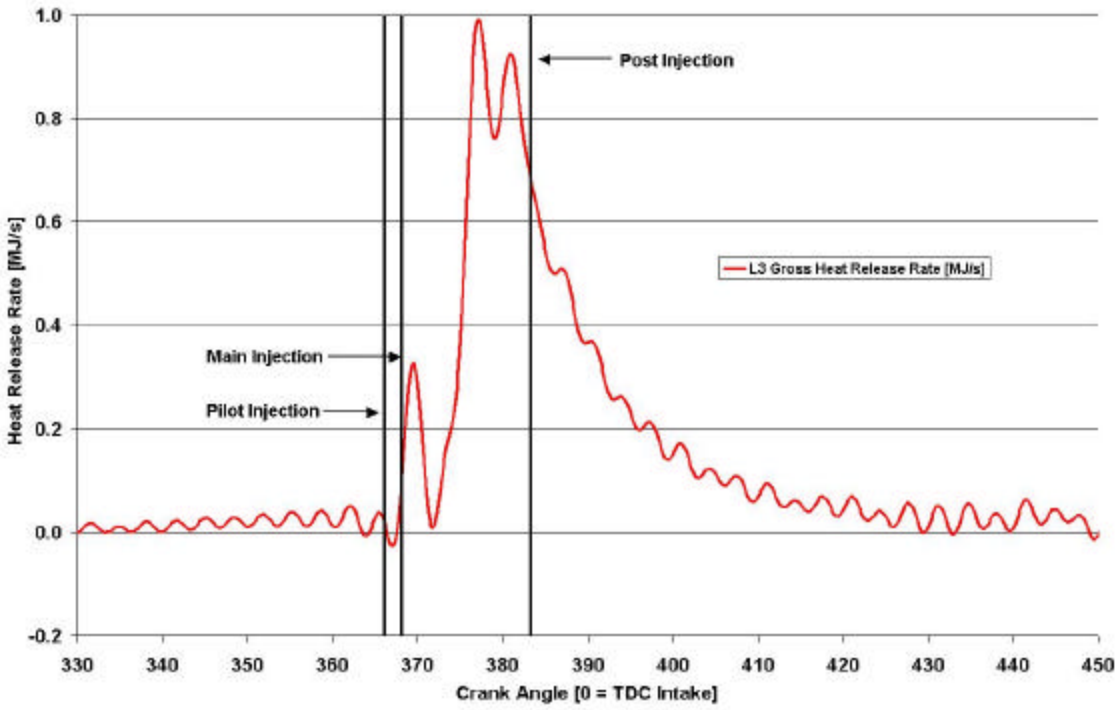

Figure 4 Event diagram for low-load (25%), injection 7° retarded from stock setting and stock EGR rate

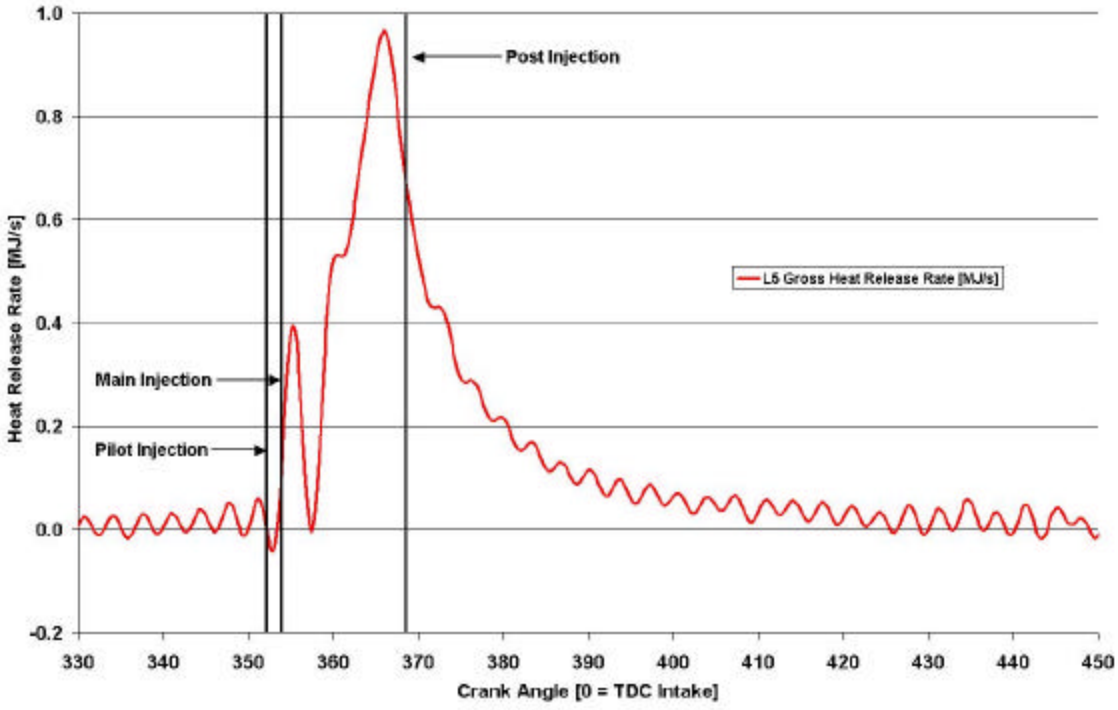

Figure 5 Event diagram for low-load (25%), injection 7° advanced from stock setting and stock EGR rate

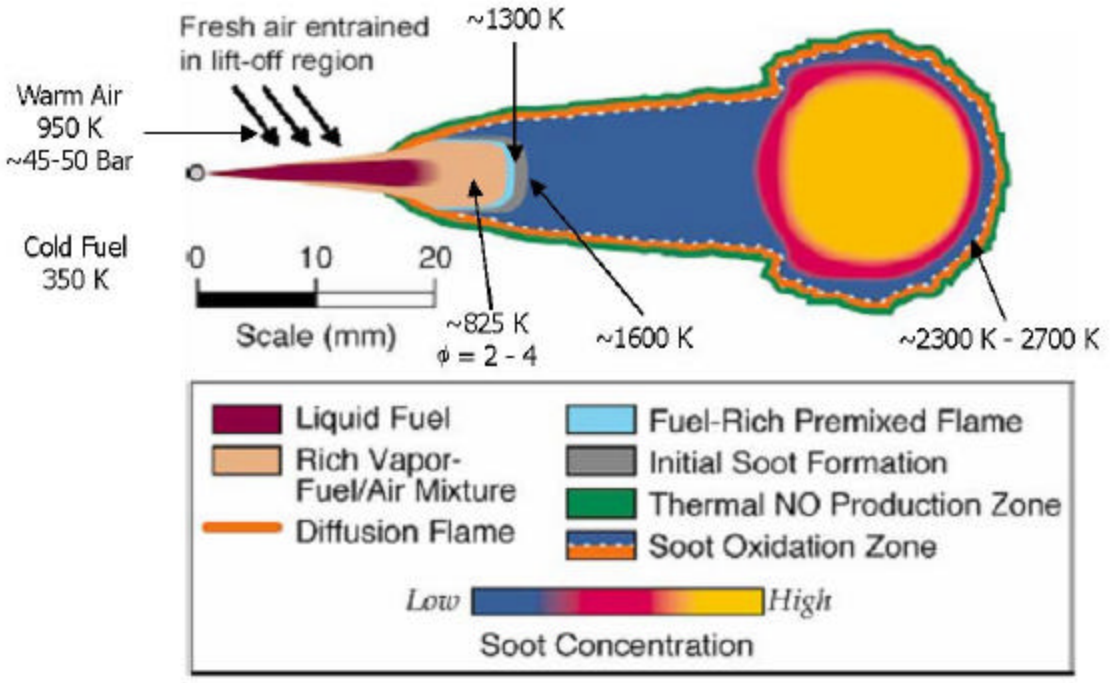

Figure 6 Schematic of new phenomenological model of diesel combustion with proposed temperatures throughout the developing plume. Adapted from [22] and [25]

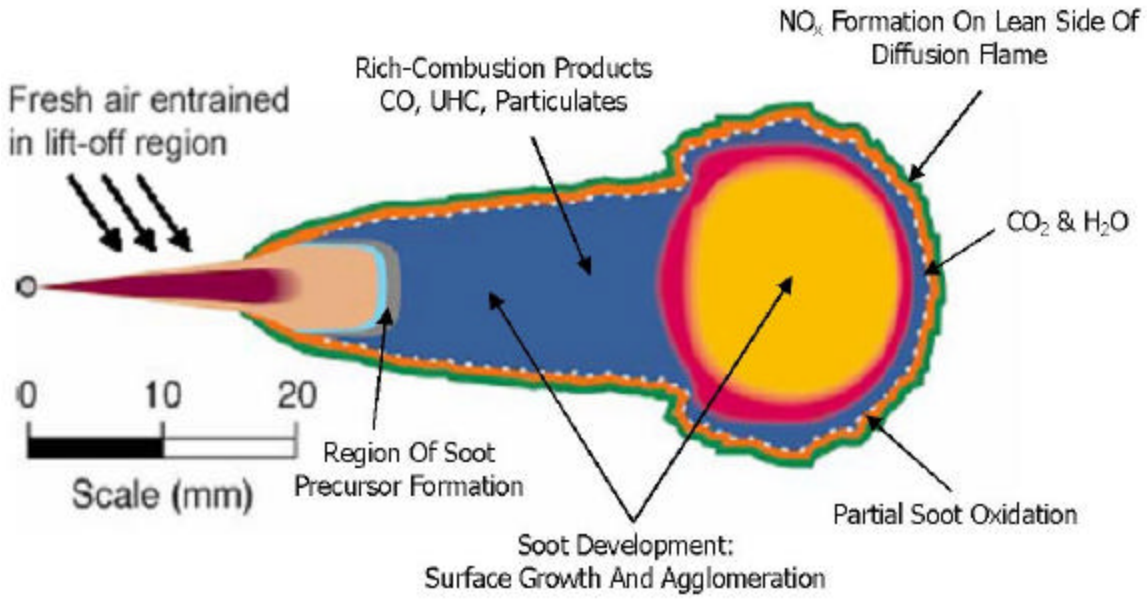

Figure 7 Schematic of new phenomenological model of diesel combustion showing spatial distribution of combustion products.

Ignition Delay

The ignition delay in diesel combustion is defined as the time between the start of injection and the start of combustion. One of the main factors governing the ignition delay in diesel combustion is the cetane number (CN) of a fuel. Although the magnitude of ignition delay is usually only described chemically through a fuel's (CN), physical processes and conditions inside the combustion chamber are equally important in determining the ignition delay.

Experiments done in constant-volume bombs, steady-flow reactors, and in rapid-compression machines have been used to study the autoignition characteristics of fuel-air mixtures . The ignition delay data from experiments carried out in these different combustion configurations can all be correlated by an Arrhenius-type equation of the following form:

$$t_{id} = Ap^{-n} \exp\left(\frac{E_A}{\tilde{R}T}\right)$$

where τ_{id} is the ignition delay; A and n are constants that depend on the fuel, injection, and air-flow characteristics; p is the cylinder pressure; E_A is the apparent activation energy for a fuel to autoignite; $\tilde{R}$ is the universal gas constant; and T is the cylinder temperature. Based on **Error! Reference source not found.**'s Arrhenius form, temperature plays a significant role in determining the ignition delay. Additionally, in the above equation, representative values of n can range from between 1 – 2 16, clearly showing that cylinder pressure can have large effects on ignition delay.

A more sophisticated version of Equation 8.1, taking into account cylinder conditions, is given by :

$$t_{id}(CA) = (0.36 + 0.22\overline{S}_p)\exp\left[E_A\left(\frac{1}{\tilde{R}T} - \frac{1}{17{,}190}\right) + \left(\frac{21.2}{p - 12.4}\right)^{0.63}\right]$$

where $\overline{S}_p$ [m/s] is the mean piston speed, T [Kelvin] and p [bars] are the charge temperature and pressure during the ignition delay (taken as TDC conditions),

In this equation, the importance of a fuel's cetane number is correlated by [16]:

$$E_A = \frac{618{,}840}{CN + 25}$$

Thus, as expected, as a fuel's CN rating increases, the required activation energy required for autoignition drops, reducing the ignition delay for a given temperature and pressure. Furthermore, the exponential dependence of ignition delay on cylinder temperature is still evident.

Modern fuel-injection technology gives engine designers precise control of fuel delivery, allowing for injection rate shaping and multiple injections per cycle. The test engine used to run experiments is equipped with a Bosch common-rail system, allowing Cummins engineers to use a multiple-injection fueling strategy. According to Cummins engineers, pilot injection is used nowadays to reduce the typical diesel "knocking" sound for societal benefits. Pilot injection accomplishes this by reducing the amount of fuel that autoignites in the initial premixed burn fraction, decreasing the sudden pressure rise that is associated with the diesel-engine sound. The small amount of fuel (1 mg/stroke in all experiments) injected a few degrees before the main injection event occurs starts the autoignition chemistry, helping to bring the prevailing cylinder conditions into a more favorable state once the main fuel is injected, reducing the overall ignition delay of the main fueling quantity.

In the burn rate analysis program used to process the cylinder pressure traces, the start of combustion (SOC) was defined as the point after the main start of injection when the heat release went through an inflection point (some conditions had two inflection points; the first was used in these cases), going from a decreasing rate in heat release to an increasing rate of heat release. The heat release drops after the start of the main injection due to the evaporative cooling effect of vaporizing fuel. Due to time constraints, the SOC was manually chosen by visually inspecting the heat-release rate curves. The behavior in the high-load, most advanced cases (H5, FTH5, H15, and FTH15) is suspect, since the SOC was difficult to pinpoint manually. Thus, the following discussions ignore these points when comparing trends.

Ignition Delay Results In Low-Load Tests

In order to reduce overall NO_x emissions, modern diesel engines use heavily retarded timing compared to older engines. Diesel engines from the 1970s and 1980s commonly had injection timings between 20° – 30° bTDC, whereas nowadays, fuel injection occurs around TDC. In the low-load experiments (~480 kPa BMEP), the stock injection timing is 1° aTDC. Since the piston is largely still near TDC, even with advanced and retarded timing, the cylinder temperatures and pressures vary little with injection timing. As compression temperatures and pressures around TDC are much higher versus conditions at 20° – 30° before TDC, the ignition delays in engines with near-TDC timing should be shorter relative to older engines, and should not vary much with injection timing.

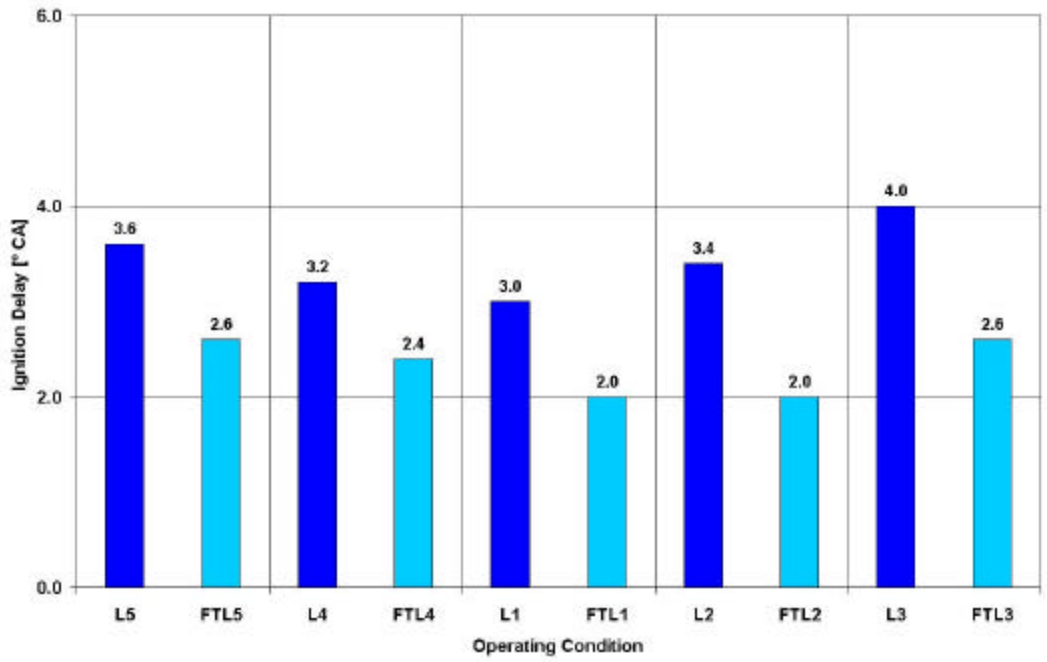

Figure 8: Ignition delay comparison between No. 2 diesel fuel and Fischer-Tropsch fuel during timing-sweep tests with stock EGR rates in low-load tests. The operating conditions are normal diesel (L1 – L5) and Fischer-Tropsch (FTL1 – FTL5). Stock timing is in the center with the most advanced timing to the left and the most retarded timing to the right.

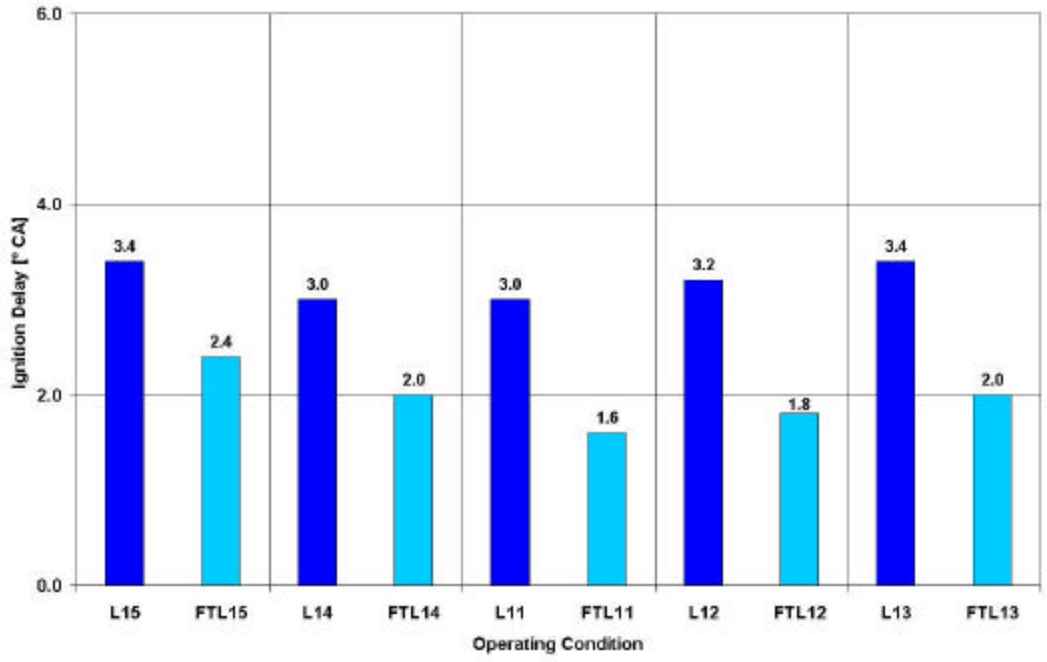

Figure 9 Ignition delay comparison between No. 2 diesel fuel and Fischer-Tropsch fuel during timing-sweep tests with increased EGR rates in low-load tests. The operating

conditions are normal diesel (L11 – L15) and Fischer-Tropsch (FTL11 – FTL15). Stock timing is in the center with the most advanced timing to the left and the most retarded timing to the right.

Ignition Delay Results in High-Load Tests

Taking into account the ± 0.2-degree resolution of the experimental setup, Figure 8.5 shows that except for the most-advanced timing condition, the ignition delays for each fuel during the high-load (~1000 kPa BMEP) experiments running with the stock-EGR rates are essentially the same ($?_d = 2.4° \pm 0.2°$) for various injection timings. Similarly, in the increased-EGR operating conditions, ignition delay values are essentially equal and equivalent to the stock-EGR conditions ($?_d = 2.4° \pm 0.2°$) for various injection timings as illustrated by Figure 8.6.

The relative insensitivity of ignition delay from 25% load to 53% load is partially due to the relative insensitivity of TDC temperatures (prior to combustion) to load. Since injection is close to TDC, the effect of timing on ignition delay is also small at high load, as at low load. For FT fuel, this is even more insensitive compared to No. 2 Diesel, since the pressure effect on ignition delay, noticeable with No. 2 Diesel, is overshadowed by temperature for FT fuel. Further implications this will be discussed with the emission trends.

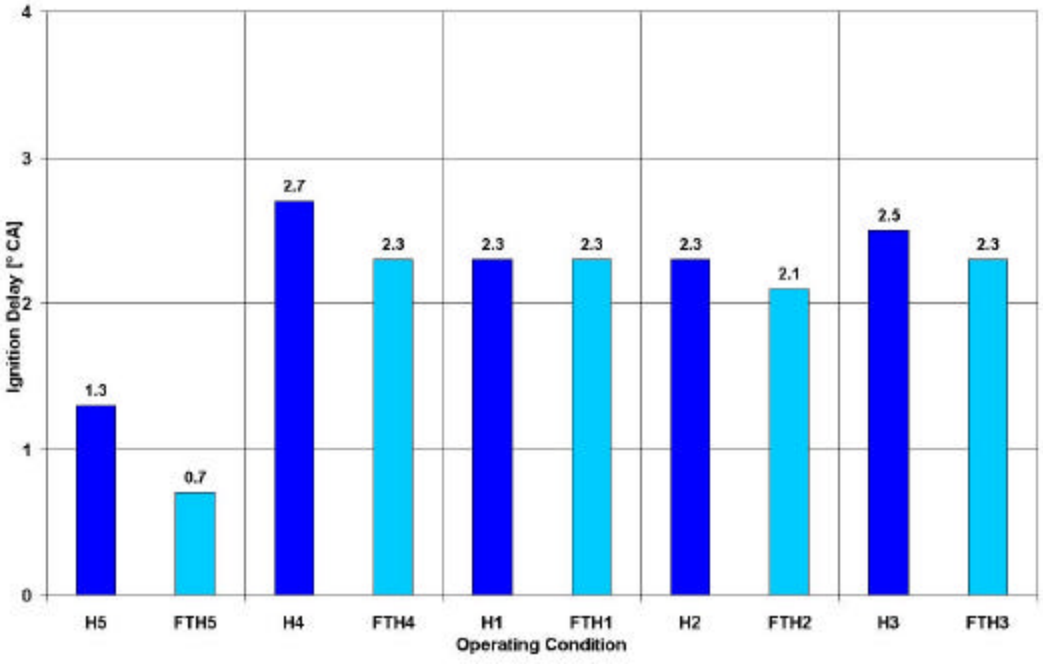

Figure 10 Ignition delay comparison between No. 2 diesel fuel and Fischer-Tropsch fuel during timing-sweep tests with stock EGR rates in high-load tests. The operating conditions are normal diesel (H1 – H5) and Fischer-Tropsch (FTH1 – FTH5). Stock timing is in the center with the most advanced timing to the left and the most retarded timing to the right. The leftmost point (H5 and FTH5) is suspect.

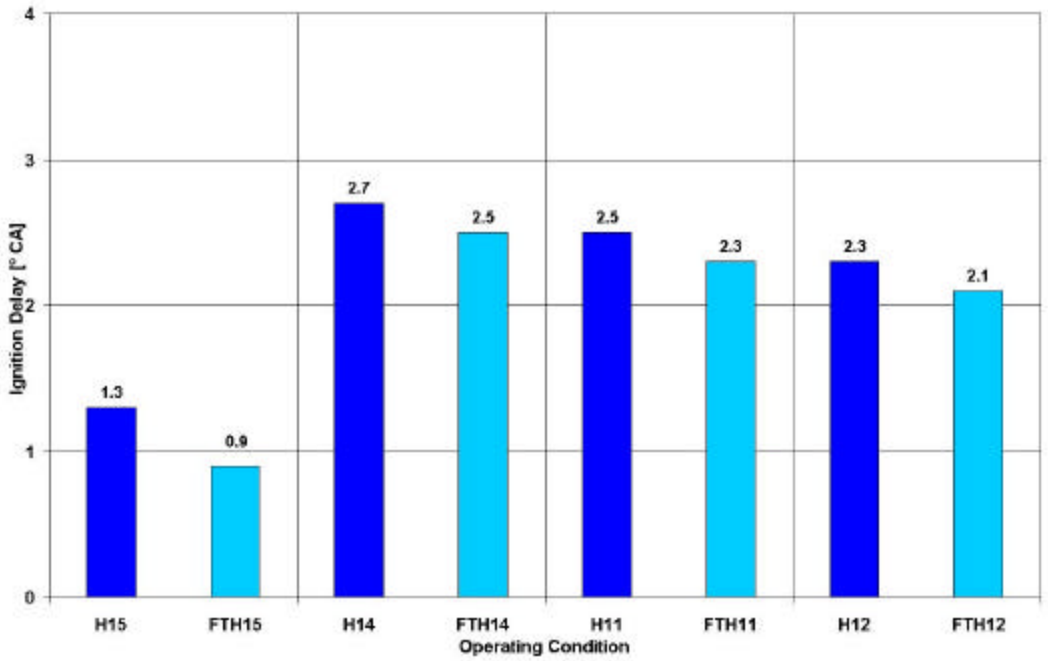

Figure 11 Ignition delay comparison between No. 2 diesel fuel and Fischer-Tropsch fuel during timing-sweep tests with increased EGR rates in high-load tests. The operating conditions are normal diesel (H11 – H15) and Fischer-Tropsch (FTH11 – FTH15). Stock timing is in the center with the most advanced timing to the left and the most retarded timing to the right. The leftmost point (H15 and FTH15) is suspect

Combustion Duration

After the ignition delay period, auto-ignition establishes the standing premixed flame. Combustion proceeds until either the fuel is completely burned or the flame is quenched. The combustion duration gives a qualitative indication of the chemical reaction rates during the two-stage oxidation of diesel fuel; long durations imply low chemical reaction rates while short durations imply high chemical reaction rates. The combustion duration referred to in the following sections is derived from the heat-release analyses of cylinder pressure traces. Combustion duration was defined as the time between the start of combustion (SOC) and the end of combustion (EOC), the EOC defined as the point of 90% of the integrated heat release. This definition of combustion duration resulted in combustion durations between about 40° – 50° at low loads and 50° – 70° at high loads (more fuel burned at high loads requires more time for combustion). Defining the EOC at locations greater than the 90% integrated heat release point resulted in abnormally long combustion durations, some points being greater than 100°. Heywood [16] suggests that fuel conversion efficiencies are highest when the combustion duration is between 40° –

50° , suggesting that the EOC definition used in the heat-release analysis program is an appropriate, although arbitrary, definition of when combustion ends.

Combustion durations results are shown below, for various timings and EGR rates for the two fuels. The major observations are summarized as follows:

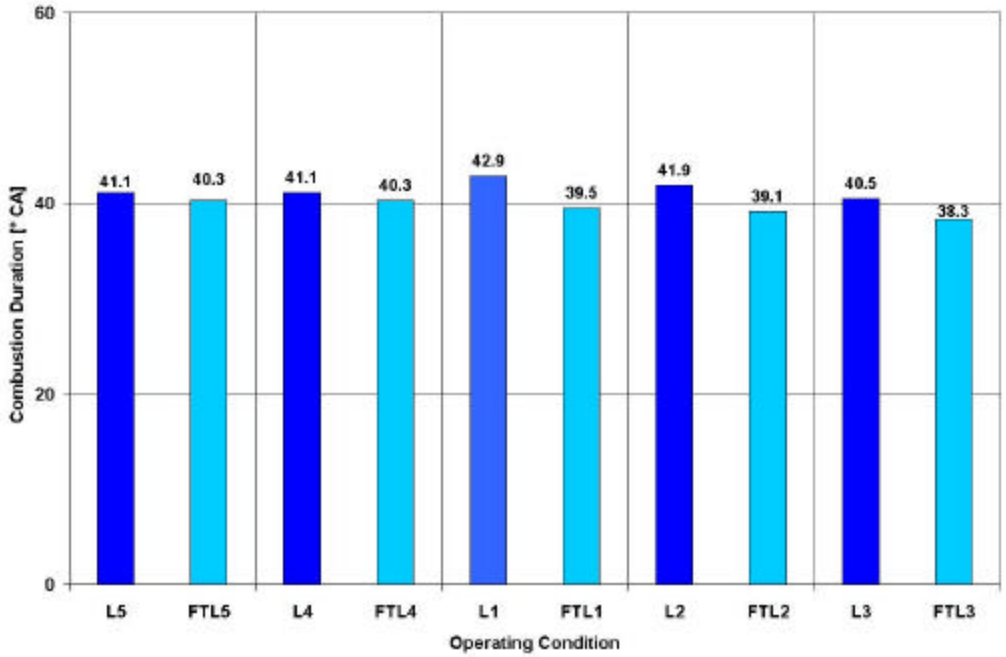

Figure 12 Combustion duration using No.2 diesel fuel and Fischer-Tropsch fuel during timing sweep test with stock EGR rates in low-load tests. The operating conditions are normal diesel (L1 – L5) and Fischer-Tropsch (FTL1 – FTL5). Stock timing is in the center with the most advanced timing to the left and the most retarded timing to the right

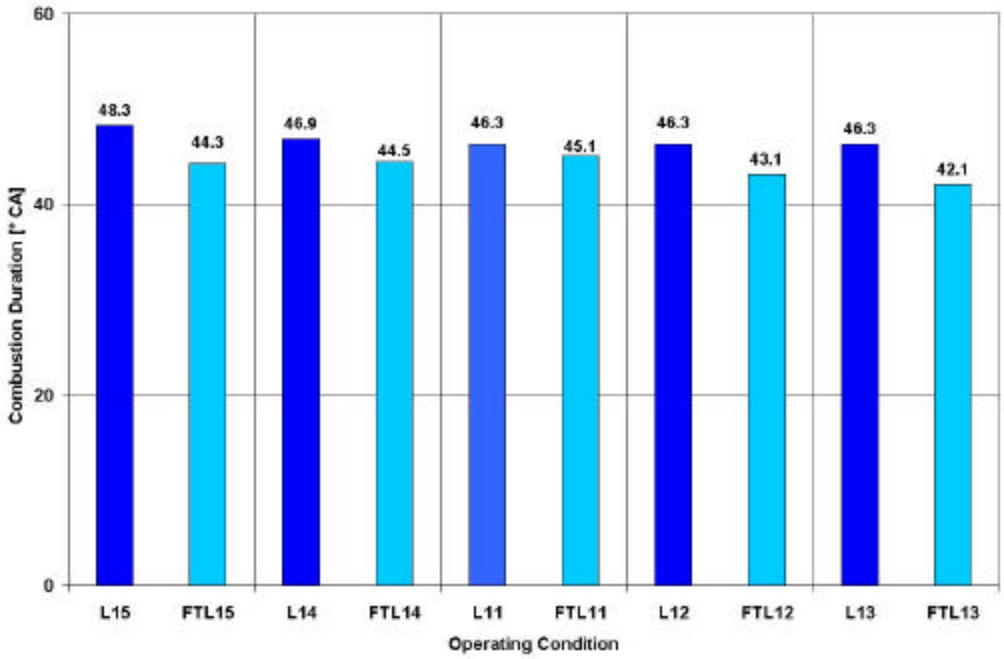

Figure 13 Combustion duration using No.2 diesel fuel and Fischer-Tropsch fuel during timing sweep test with increased EGR rates in low-load tests. The operating conditions are normal diesel (L11 – L15) and Fischer-Tropsch (FTL11 – FTL15). Stock timing is in the center with the most advanced timing to the left and the most retarded timing to the right

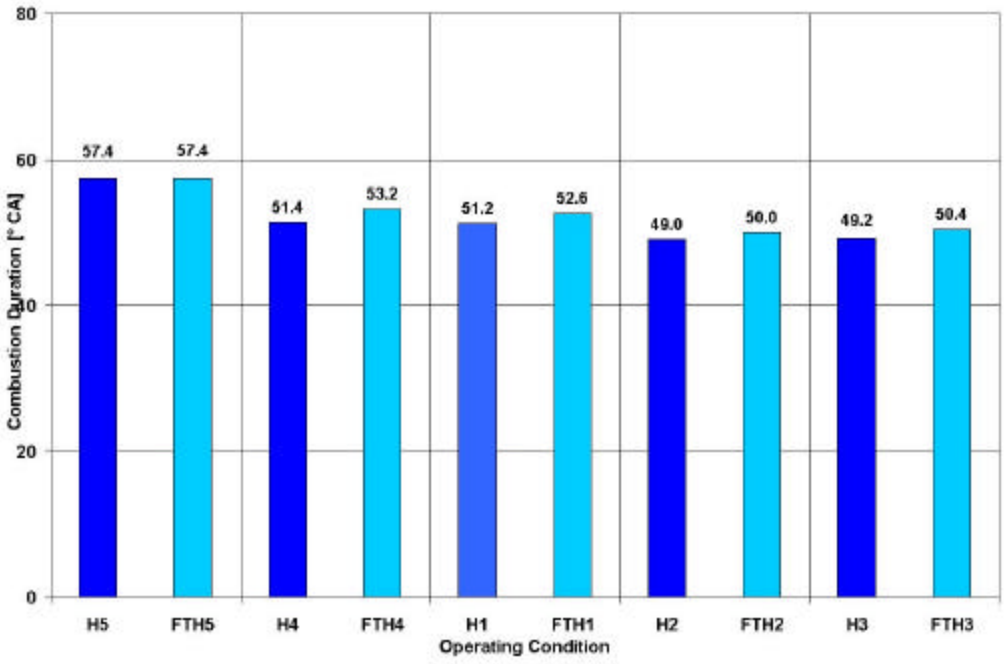

Figure 14 Combustion duration using No.2 diesel fuel and Fischer-Tropsch fuel during timing sweep test with stock EGR rates in high-load tests. The operating conditions are normal diesel (H1 – H5) and Fischer-Tropsch (FTH1 – FTH5). Stock timing is in the center with the most advanced timing to the left and the most retarded timing to the right

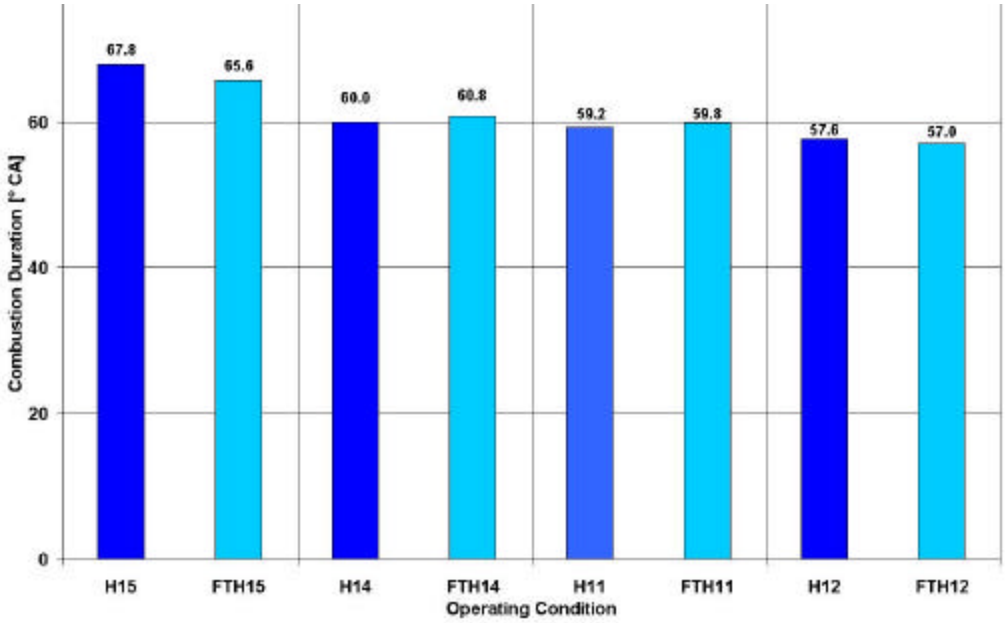

Figure 15 Combustion duration using No.2 diesel fuel and Fischer-Tropsch fuel during timing sweep test with increased EGR rates in high-load tests. The operating conditions are normal diesel (H11 – H15) and Fischer-Tropsch (FTH11 – FTH15). Stock timing is in the center with the most advanced timing to the left and the most retarded timing to the right

(a) Combustion durations for the FT fuel are general shorter than that for No.2 diesel, despite the slightly longer injection durations for the FT fuel (to account for density difference), at comparable conditions.
(b) Combustion durations are relatively insensitive to injection timings for both the No. 2 diesel and FT fuel and at each EGR condition.
(c) Combustion duration increases as EGR rate is increased. Comparing Figure 8.8 with Figure 8.7, and Figure 8.10 with Figure 8.9 [EGR changes], we see that at a constant BMEP and timing, the combustion duration increases as the EGR rate increases. The combustion duration increased from about 3° – 7° at low loads, depending upon timing, while changing from about 7° – 10° at high loads depending upon timing. This is expected since EGR acts as a diluent.

To get a better understanding of combustion development, the combustion duration is divided into three intervals describing the beginning, middle and end of combustion. In the heat release program, in addition to the 90% integrated heat release location that defined EOC, the 10% and 50% integrated heat release locations were calculated. From these points, the durations between SOC to the 10% integrated heat release point, 10% to 50% heat release points, and 50% to 90% heat release points were determined, giving further insight into the combustion duration trends.

SOC-to-10% Heat Release Duration

In order to reduce both particulate matter and NO_x output, the test engine is equipped with a common rail fuel injection system, injects fuel around TDC, and uses multiple-injection fueling strategies. As a result of these emission-reducing technologies, the test engine has shorter ignition delays compared to older engines (on a time basis, 0.2 to 0.3 ms for the test engine vs. 0.4 to 1.5 ms for high-compression ratio and turbocharged

engines [12]) along with combustion that occurs predominantly in the expansion stroke. This late phasing of combustion leads to trends not seen in older engines.

At stock EGR rates, the duration between the start of combustion to the point of 10% heat released increases as timing is retarded from the most-advanced injection timing point. Comparing No. 2 diesel and FT diesel, the SOC-to-10% heat release duration is longer for every operating condition with FT diesel. This trend is a function of a fuel's associated ignition delay and the phasing of combustion with respect to TDC. Similar trends with respect to timing (No. 2 diesel shows an insensitivity to timing until the most-retarded injection condition) and fuel type are seen with the increased-EGR operating points (see figure 17).

The SOC-to-10% heat-release duration should have an inverse relationship with ignition delay; shorter ignition delays lead to longer SOC-to-10% heat release durations. This is shown by the magnitude of the SOC-to-10% heat release durations with FT fuel. With similar trends based on phasing, FT fuel shows prolonged SOC-to-10% heat release durations compared to Number 2 diesel fuel at the same operating condition. This occurs due to FT fuel's higher CNI rating versus Number 2 diesel fuel, which implies less air entrainment and lower initial reaction rates when using FT fuel.

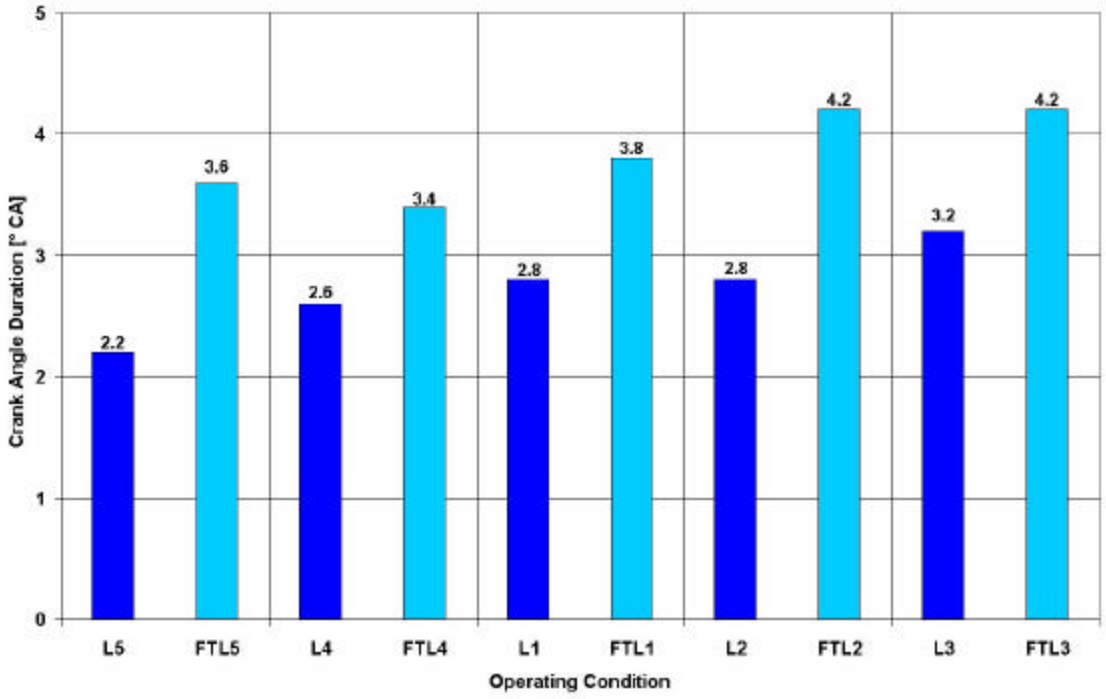

Figure 16 SOC-to-10% durations using No.2 diesel fuel and Fischer-Tropsch fuel during timing sweep test with stock EGR rates in low-load tests. The operating conditions are normal diesel (L1 – L5) and Fischer-Tropsch (FTL1 – FTL5). Stock timing is in the center with the most advanced timing to the left and the most retarded timing to the right.

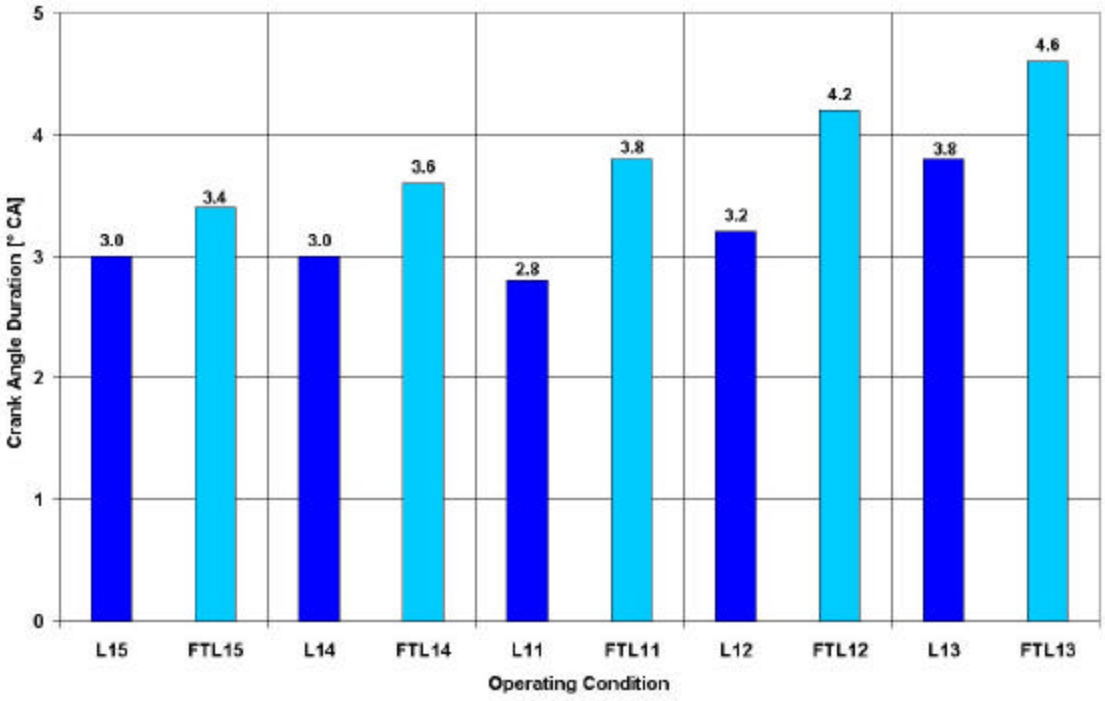

Figure 17 SOC-to-10% durations using No.2 diesel fuel and Fischer-Tropsch fuel during timing sweep test with increased EGR rates in low-load tests. The operating conditions are normal diesel (L11 – L15) and Fischer-Tropsch (FTL11 – FTL15). Stock timing is in the center with the most advanced timing to the left and the most retarded timing to the right.

10%-to-50 Heat Release Duration

Compared to heat release rate curves common to older engine technology, the heat release rates of the modern engine used in this study are drastically different. The figures show that the longer ignition delays in older engines result in a large initial peak, meaning a considerable amount of fuel underwent auto-ignition in the initial premixed burn. These curves suggest that the majority of the initial heat release is controlled by the auto-ignition event in older engines. Heat release profiles (see Figure 8.15 and Figure 8.16) from the model year 2002 (MY02) engine at MIT show that at the initial peak common in older engines is virtually non-existent, the only evidence that auto-ignition occurs is the change in slope as the curve rises to a single peak. Therefore, the diffusion flame dominates the initial heat release in a modern diesel engine.

Since the diffusion flame in a diesel engine burns stoichiometrically, or very close to stoichiometric, its adiabatic flame temperature is very high, ranging from 2300 K – 2700 K [25] depending upon initial conditions. However, the adiabatic flame temperature of a rich premixed flame can be quite low, and researchers suggest that the rich fuel-air mixture in a diesel fuel jet can range from 825K – 1600 K [25]. Therefore, once the diffusion flame establishes, the rate of heat release will completely dominate over that of the premixed flame.

Since the flame lift-off point delineates where the Damköhler number is of order magnitude one, the initial rate of reaction in the diffusion flame will be controlled by the amount of fuel-air mixing, dictated by the pressure difference across the nozzle during injection. Since the injection pressure in modern diesel engines is substantially higher than the peak pressures seen during combustion, the initial rate of heat release following the establishment of the diffusion flame will be mostly dependent upon the injection pressure. Therefore, the near-constant 10%-50% heat release durations shown in Figure 8.17 with both No. 2 diesel (8.8° ± 0.4°) and FT fuel (8.4° ± 0.2°) is expected.

50%-to-90% Heat Release Duration

Figure 23 shows that the 50%-to-90% heat release duration decreases as injection timing is retarded beyond TDC. Combustion rates must therefore be increasing since the amount of fuel injected into the cylinder to keep the BMEP constant increases as combustion is phased later in the expansion stroke. To increase the chemical reaction rates in diffusion flames, the diffusion-flame-rate characteristics must be improved (laminar burning velocity and/or thermal diffusivity) through changes in ambient conditions, reactant mixture state (equivalence ratio, temperature and pressure), and/or the extent of bulk motion mixing the fuel and oxidizer. For combustion phased towards the expansion stroke, the prevailing cylinder conditions diminish the burning velocity (the effect of the drop in temperature supersedes the effect of the drop in pressure). Thus, either the mixing of fuel and oxidizer is improving or the unburned mixture is reaching a more reactive state as the piston moves away from TDC. These changes in combustion (50-90% burn) rates way into the expansion stroke have important ramification in the observed emission behavior.

The data shown in Figures 23 are for the stock EGR rates. At the higher EGR rate, the trend with injection timing and the fuel effects affecting the latter part of combustion are similar.

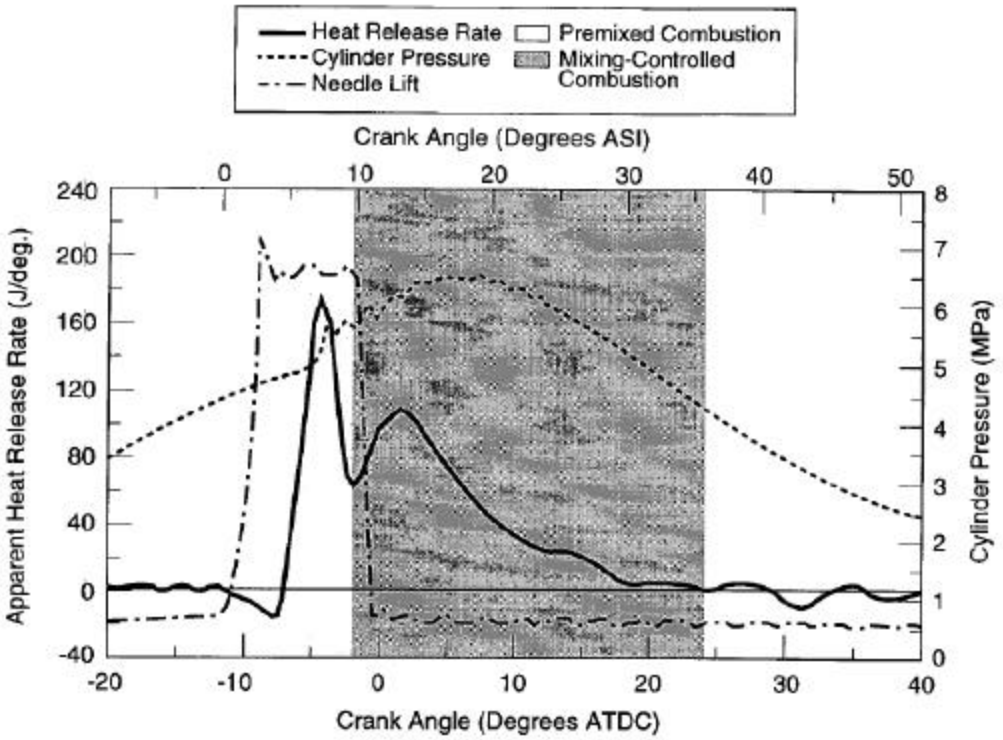

Figure 18 Heat release typical of older diesel engine technology.

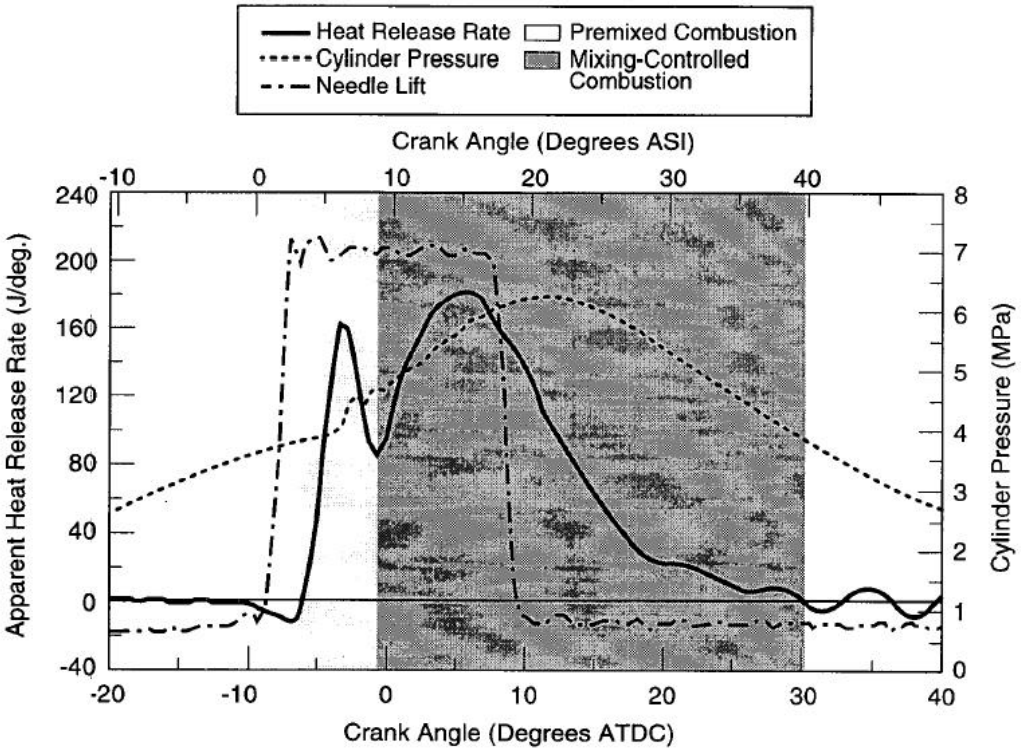

Figure 19 Heat release typical of older diesel engine technology. High-loads. Figure 8b [22].

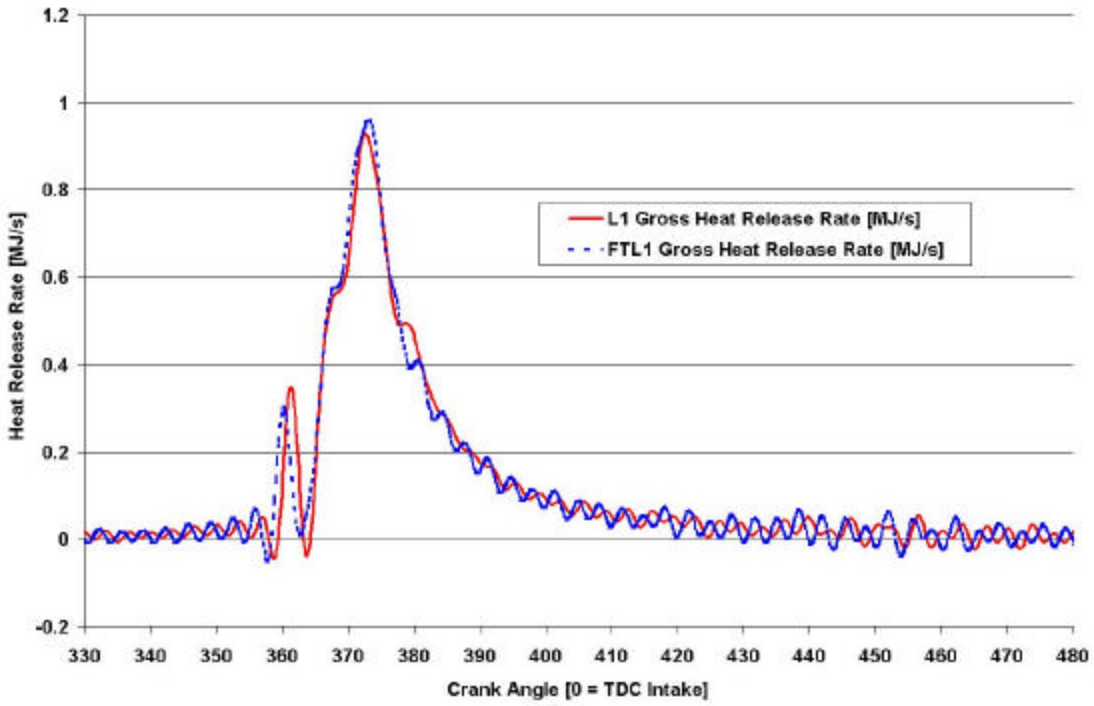

Figure 20 Heat release of Clean Diesel engine at MIT at low load with stock timing and EGR rate. Solid line applies to operation with No. 2 diesel, dotted line is for FT fuel.

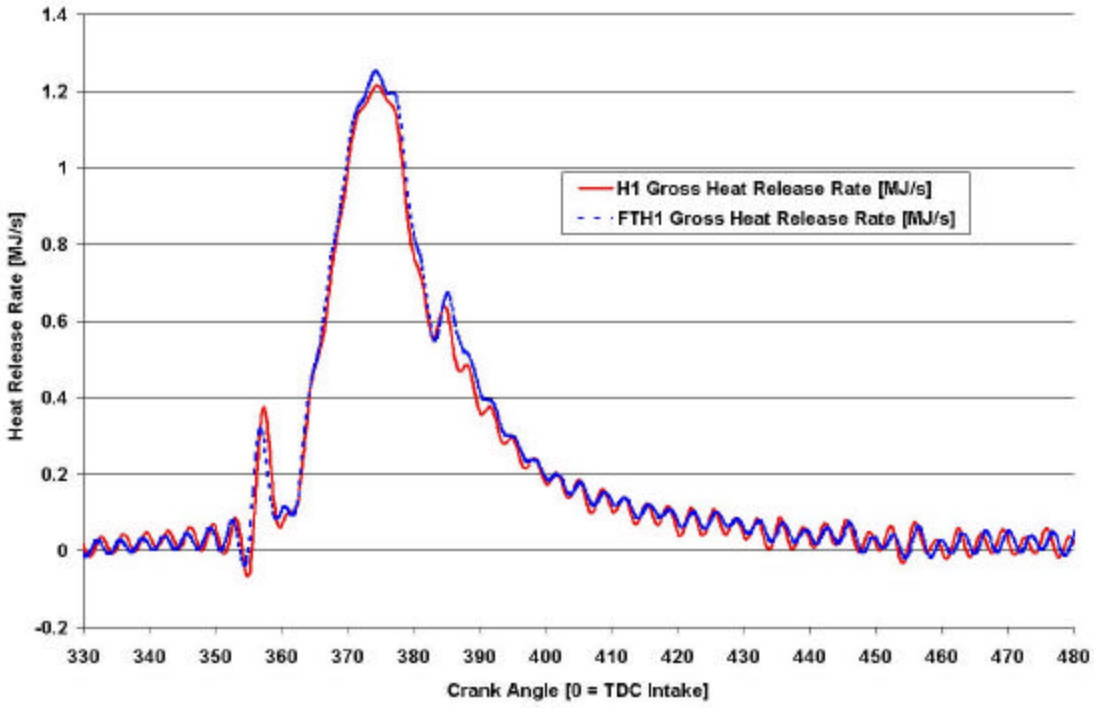

Figure 21 Heat release of Clean Diesel engine at MIT at high load with stock timing and EGR rate. Solid line applies to operation with No. 2 diesel, dotted line is for FT fuel.

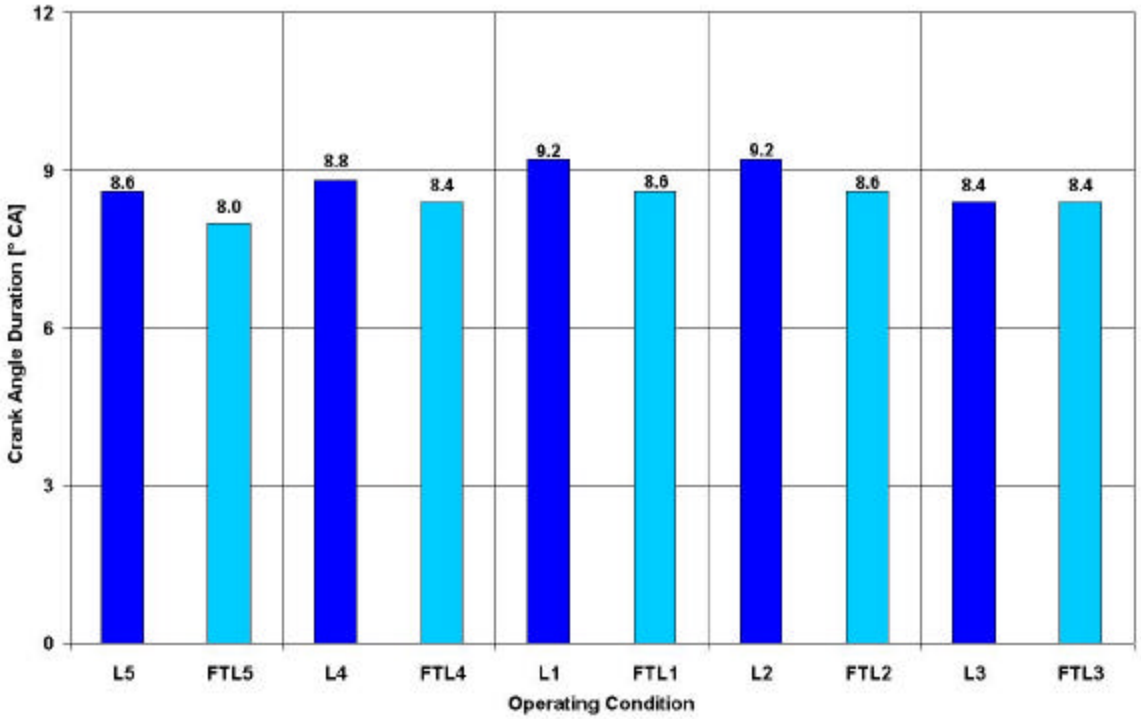

Figure 22 10%-to-50% heat release duration in Modes L1 – L5 and FTL1 – FTL5

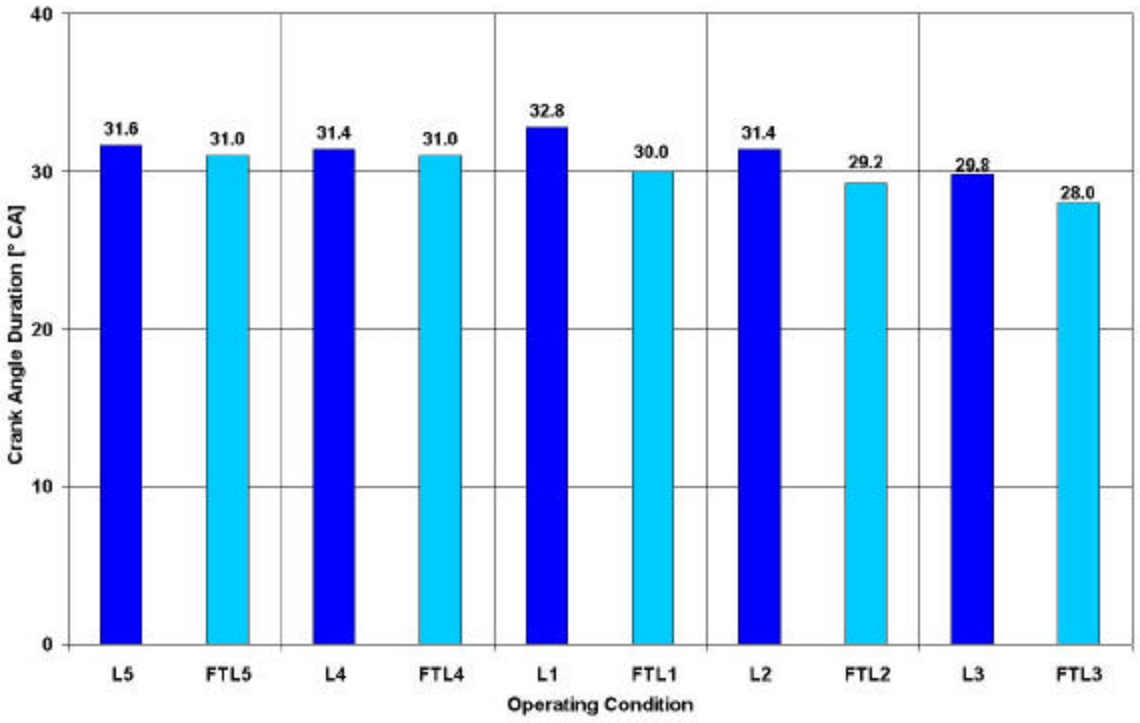

Figure 23 50%-to-90% heat release duration in Modes L1 – L5 and FTL1 – FTL5

Combustion Duration Behavior and Fuel Properties

The results in the previous sections show that, at low load, the overall combustion duration is shorter for the FT fuel compared to the No. 2 diesel. First, the SOC-to-10% burn duration takes longer with FT fuel. Next, the 10%-to-50% burn duration was essentially constant for a given fuel and differences between fuels were slight due to physical mixing dominating the combustion rate in the initial inception of the diffusion flame. Therefore, the decrease in overall burn duration due to fuel properties must be related to behavior at the end of combustion (50-90%), which favor a faster burn for FT fuel late in the expansion stroke.

The conceptual model is as follows: In general, as combustion is phased later in the expansion stroke, the temperature of the ambient unburned gas decreases. As fuel is still being injected into the cylinder up until around the point of 50% heat release in both low- and high-load tests, the drop in cylinder temperature affects the auto-ignition chemistry of fuel at the end of injection. As CN increases, the sensitivity on ambient temperature before auto-ignition occurs is lessened. Therefore, especially with combustion phased in the expansion stroke, late-injected fuel of high CN, such as the FT fuel, competing

against the motion of the piston that is extracting work and cooling the gases, can still auto-ignite relatively quickly to maintain a reasonable rate of combustion. This is clearly evident in Figure 8.18, which show that the 3°- and 7°-retard conditions show the largest differences in 50%-to-90% heat release durations, versus timing near TDC.

Comparing the two fuels at high loads, except for the advanced-timing, high-EGR point, the combustion durations were essentially the same, or varied only slightly. The insensitivity of the burn duration to fuel type at a specific condition at high loads is attributed to the increase of the overall cylinder temperature and injection pressure that promote mixing and reduce the time before auto-ignition.

General Heat Release Trends Between Number 2 Diesel and FT Fuel

In order to meet current EPA emission requirements, the test engine uses a high-pressure common-rail fuel injection system, retarded fuel-injection strategies, a cooled EGR system, and a VGT turbocharger. The implementation of the first two aforementioned emission-reducing methods results in heat release characteristics in modern engines that differ substantially from older engines. In general, compared with Figure 8.13 and Figure 8.14, the heat release graphs do not exhibit the usual dual-peak heat release characteristic. The small spike before the large heat release portion in the graphs is due to the pilot injection of the overall fueling strategy. It does not correspond to the initial premixed burn fraction as only about 3% or less of the fuel is injected during the pilot injection. The lack of an initial, premixed burn peak is a function of the small ignition delays and increased injection pressures that reduce the size of the initial fuel-rich mixture that autoignites. Thus, as the majority of the fuel is burned in a diffusion flame, usually one peak persists, although premixed burn peaks are sometimes present depending the degree of injection retard, as evinced by the aforementioned figures.

At low loads and stock EGR rates, FT fuel has higher maximum heat release rates, versus No. 2 diesel fuel. The location of maximum heat release is similar for both fuels, occurring slightly before the point of 50% heat release. The heat release data is consistent with a conceptual model that the FT's higher CN allows for a more rapid autoignition of late-injected fuel at the tail end of combustion, where the unburned gases are cooling from the downward motion of the piston.

At low loads with increased EGR rates, the difference in maximum heat release rates is suppressed for more advanced timings. The overall-higher gas temperatures reduce the effect of FT fuel's CNI advantage, closing the gap between the maximum heat release rates. On the other hand, at advanced timings, the FT fuel's CNI advantage affects more strongly the start of combustion. The retarded injection timings show increasingly larger differences between the two fuels in burn rates, again based on the fact the higher CNI rating of FT diesel fuel allows for faster oxidation even as the cylinder contents have cooled due to the late SOC. The slight reduction in the maximum rate of heat release in some timing conditions as EGR is increased is due to the rise in the burned gas fraction that is know to decrease the laminar burning velocity [16]. Since the composition of

EGR at low loads still contains a considerable amount of excess air, the oxygen concentration does not drop by much when EGR is increased, only slightly affecting the rate of reactions in the diffusion flame.

In general, the heat release curves for FT diesel show that the heat release rate races to a peak sooner than No. 2 diesel, due to the reduced ignition delay times with FT fuel at low loads. Also, although the maximum heat release rates for FT fuel are different from No. 2 diesel at the low load conditions discussed above, the general shape and characteristics of the heat release curves for each operating condition are essentially the same. These suggest that the oxidation pathways for each fuel are not drastically different [5]. Of note, however, are the most-retarded injection timings at stock and increased EGR rates (Modes L3, FTL3, L13, and FTL13). As combustion in these conditions is phased furthest away from TDC, fuel is injected into increasingly cooler conditions, making autoignition chemistry more important. The No. 2 diesel heat release rate approaches the behavior of the classical heat release shape, at the most retarded timing conditions, as two peaks are clearly evident, supporting the fact that the initial and standing premixed flame are increasingly important due to the low CN number rating of the fuel. Under the same engine conditions with FT fuel, the peak due to the premixed flame is heavily reduced in magnitude, again a function of FT fuel's higher CNI rating.

Emissions Characteristics

Due to the overall-lean operation of diesel engines, carbon monoxide (CO) levels are negligible. Tthe compression of only air during the compression stroke prevents several major sources of unburned hydrocarbons (UHC) common in pre-mixed engines, thus UHC from diesels are usually within acceptable levels. Therefore, the following discussion focuses primarily on oxides of nitrogen ($NO_{x)}$ and particular matter (PM) emission behavior in the experiments.

NO_x Emission Trends with Engine Operating Characteristics

As shown in Figure 8.19, NO_x output is a strong function of injection timing. This well-known trend is a function of the peak gas temperatures during combustion. Peak cylinder pressure and temperature increase appreciably as injection timing is advanced from the stock timing point while noticeable temperature reductions occur as timing is retarded. Since the predominant NO_x-formation mechanism in diesel engines is thermally driven, NO_x emissions should scale with peak cylinder temperatures. Interestingly, the gas temperatures in the exhaust manifold show the opposite trend with timing, lower temperatures in advanced timing with higher temperatures in retarded timing, beyond TDC. As combustion occurs later in the expansion stroke, less work is extracted per crank angle due to the thermodynamic reduction in efficiency with cooler working fluids, resulting in elevated exhaust gas temperatures.

The results also show that NO_x output is also strongly dependent upon EGR rates. Increasing EGR was effective in decreasing brake specific NO_x for both fuels at every operating condition. At the 50 percent load point, NO_x outputs dropped from 22% – 32% when increasing EGR rates from the reduced- to stock-EGR set points. Increasing EGR from the stock setting, NO_x outputs dropped from 38% – 46% at high loads.

EGR effectively reduces NO_x in two distinct ways. Similarly to SI engines, EGR acts as a diluent with added heat capacity, helping reduce peak gas temperatures. More importantly for diesel engines, especially at high loads, EGR reduces the amount of oxygen available. As the fuel-air equivalence ratio increases towards the stoichiometric value, the mole fraction of oxygen steadily decreases while the mole fractions of both carbon dioxide (CO_2) and water vapor (H_2O) steadily increase in the exhaust-gas composition (see Figure 8.20). Furthermore, as the exhaust gas is composed of more polyatomic species, the heat capacity increases (based on the Kinetic Theory of Gases), shown by a related decrease in $\gamma_{exhaust}$ as the fuel-air equivalence ratio becomes richer (see Figure 26).

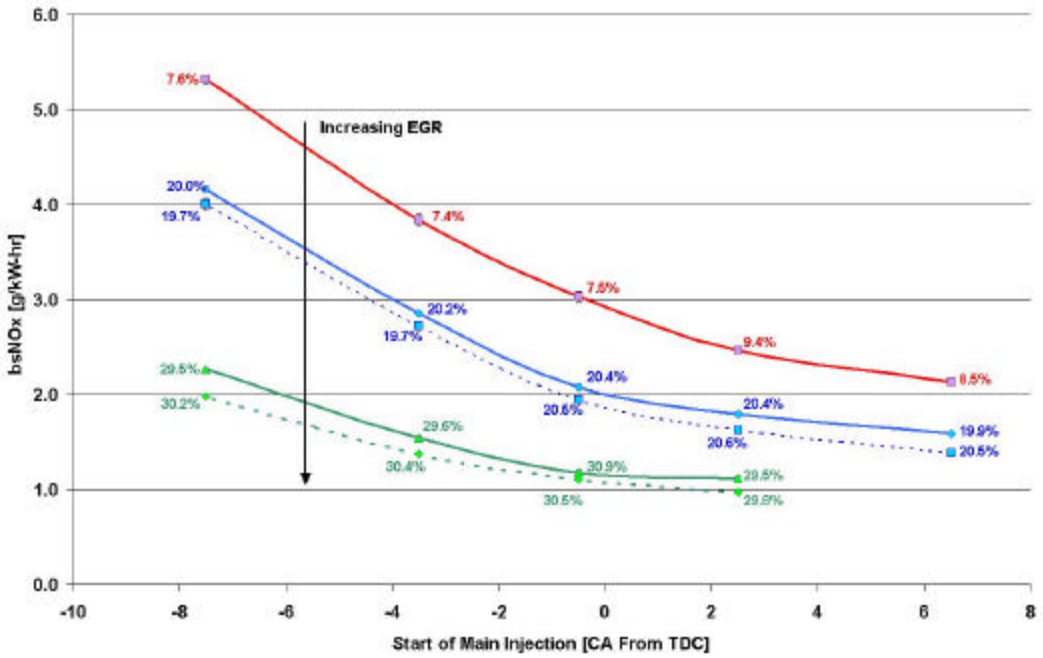

Figure 24 Brake-specific NO_x ($bsNO_x$) emissions versus the start of main injection timing for all experimental conditions at high loads. Solid lines apply to No. 2 diesel fuel and dashed lines apply to FT fuel. The individual data labels report the EGR rates for each condition while the error bars show the error for ± 1 S.D. Stock timing points are the middle points

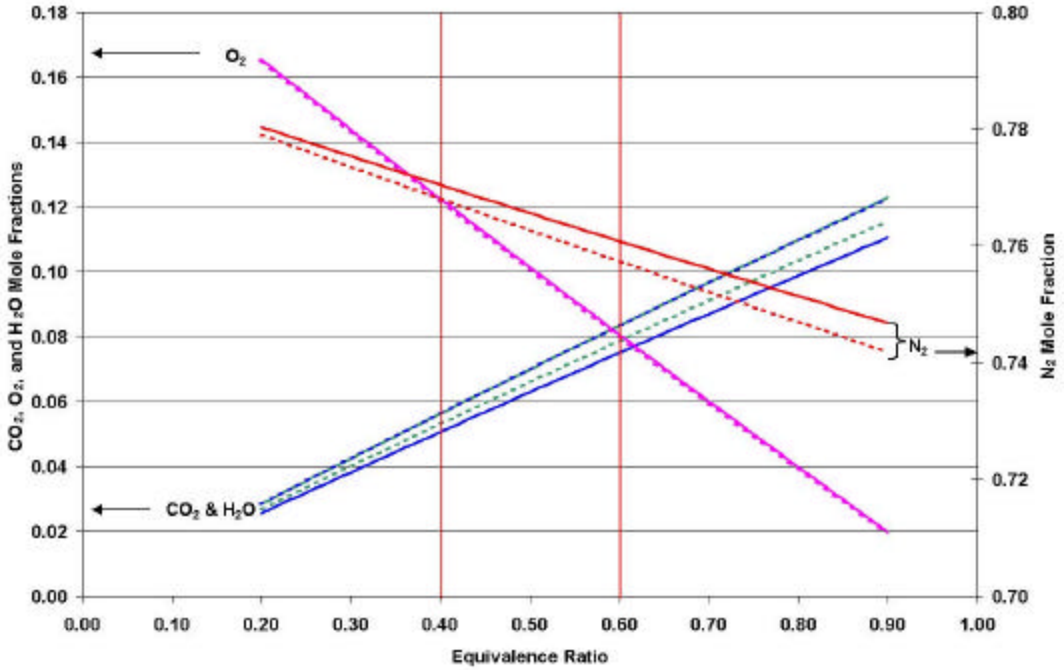

Figure 25 Exhaust gas composition versus fuel-air equivalence ratio for No. 2 diesel fuel and FT fuel. Mole fractions are based on No. 2 diesel fuel composition of ($CH_{1.80}$) and FT fuel composition of ($CH_{2.12}$). Solid lines pertain to No. 2 diesel fuel while dotted lines are for FT fuel. For CO_2 and H_2O lines, lower solid line is H_2O mole fraction for No. 2 diesel, while lower dashed line is CO_2 mole fraction for FT

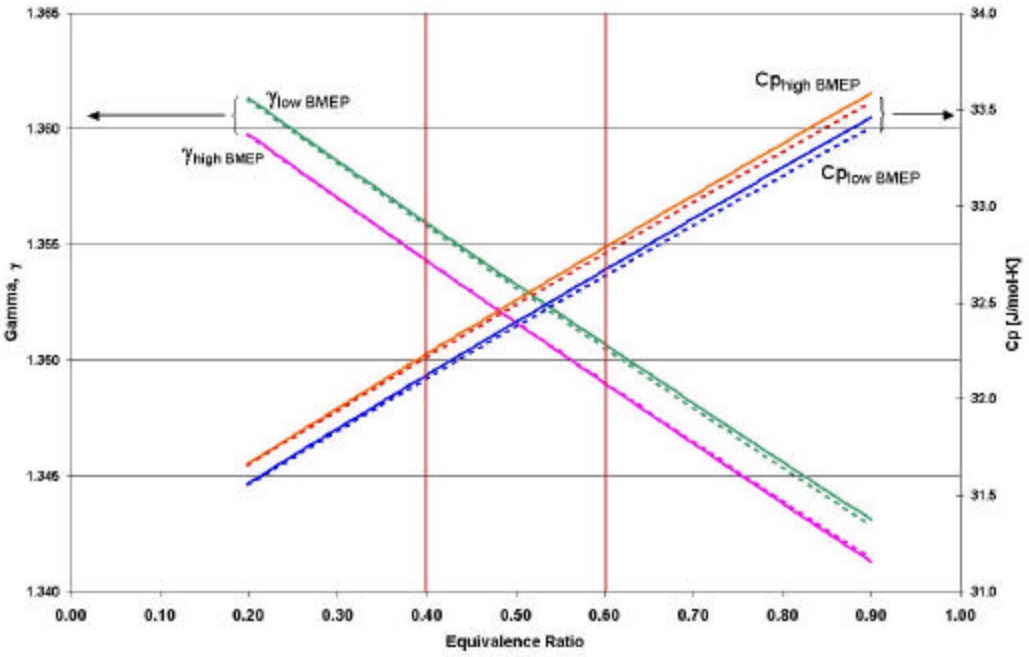

Figure 26 Ratio of specific heats of exhaust gas ($\gamma_{exhaust}$) versus fuel-air equivalence ratio of reactants. Mole fractions are based on No. 2 diesel fuel ($CH_{1.80}$). and FT fuel composition of ($CH_{2.12}$). Solid lines pertain to No. 2 diesel fuel while dotted lines are for FT fuel

NO_x Emission Trends with Fuel Properties

Compared to No. 2 diesel, FT fuel consistently reduces NO_x emissions at all timing points at high loads, while at load loads, the NO_x data seem to be very similar. Comparing NOx values for both fuels at the increased EGR rates shows that from the stock injection timing to the most-retarded timing condition, the NO_x values are almost constant, while both fuels show NO_x increases as timing in advanced, less so for the FT fuel.

An explanation of this behavior is suggested by Lee et. al [28]. It was reported that the H/C ratio of a fuel can also impact NO_x emissions by influencing another aspect of the kinetic pathway through reductions of the concentration of species required by the rate-limiting step in the extended Zeldovich mechanism. As shown in Figure 8.20, the mole fraction of water in the exhaust gas of FT fuel is slightly higher than No. 2 diesel fuel due to its higher H/C ratio. It was proposed that since water has a lower tendency to dissociate at high temperatures compared to carbon dioxide, fuels with higher H/C ratios will have lower concentrations of radicals, reducing the kinetic production of NO_x as it relies on radical-oxygen concentration. Furthermore, Figure 8.20 shows that the concentration of nitrogen is lower for the high-H/C ratio FT fuel. Again, a reduction in nitrogen concentration should reduce the production rate of NO_x. Although the above arguments should also apply to the low-load tests, the difference in H_2O and N_2 mole fractions between FT fuel and No. 2 diesel fuel decreases as the overall fuel-air equivalence ratio decreases, while the mole fraction of oxygen rises substantially as conditions become more lean. As such, the importance of H_2O dissociation decreases as the radical-oxygen contribution from molecular oxygen takes precedence.

Particulate Matter Emission Trends with Engine Operating Characteristics

Figure 27 shows the low-load brake-specific particulate matter (bsPM) behavior from the modern 2002 Cummins ISB engine, which is quite different from that of earlier models. In any case, the particulate matter from FT fuel is greatly reduced from that of No.2 diesel. Traditionally, particulate matter levels reach a minimum as timing is optimized for a specific load, speed, and EGR rate. However, the low-load trends show that the PM output of the test engine actually had locally-maximized PM outputs at the factory injection timing settings and at timings close to TDC (Modes L4 and FTL4) while PM levels drop as injection timing is moved away from TDC.

The particulate matter that exits the engine is based on two competing processes, the extent of particualte formation and oxidation. Many models for soot formation and oxidation exist [29], ranging in scope from empirical, semi-empirical, and detailed-chemistry formulations. Empirical models are relatively crude, as they do not separate

formation and oxidation in their prediction of soot while detailed-chemistry models came become overly complex. A commonly used semi-empirical model in diesel engines considers the overall soot mass formation rate, $\frac{dM_s}{dt}$, as function of the formation rate, $\frac{dM_{sf}}{dt}$, and oxidation rate, $\frac{dM_{so}}{dt}$, considered separately from one another:

Equation a
$$\frac{dM_s}{dt} = \frac{dM_{sf}}{dt} - \frac{dM_{so}}{dt}$$

Equation b
$$\frac{dM_{sf}}{dt} = A_f M_{fv} p^{0.5} \exp\left(\frac{-E_f}{\tilde{R}T}\right)$$

Equation c
$$\frac{dM_{so}}{dt} = A_o M_s x_O p^{1.8} \exp\left(\frac{-E_o}{\tilde{R}T}\right)$$

In Equation a, A_f is the pre-exponential factor for soot formation, M_{fv} is the mass of fuel vapor, and E_f is the activation energy for soot formation. In Equation b, A_o is the pre-exponential factor for oxidation, M_s is the mass of soot, and x_O is the mole fraction of molecular oxygen. Common to both rate equations are the pressure and temperature of the cylinder, p and T, along with the universal gas constant. The formation and oxidation rate equations proposed by Hiroyasu are both Arrhenius-type rate equations with activation energies of $E_f = 8x10^4$ kJ/mol for formation and $E_o = 12x10^4$ for oxidation. The magnitudes of each make sense since formation occurs at lower temperatures than oxidation, so its activation energy should be lower.

Based on the fact that higher peak cylinder pressures and temperatures lead to increasing NO_x as injection timing is advanced, the overall PM output is most likely a difference of two large numbers as formation and oxidation rates are likely elevated. Since PM drops as the cylinder gets hotter, the oxidation rate is most likely dominating as injection timing advances, leading to the drop in PM shown in the data. Combine this with the fact that the combustion duration grows with injection timing advance, and the time for PM oxidation increases helping to lower the overall engine-out PM level.

As combustion is phased after TDC, the overall cylinder conditions become cooler as the piston expands the cylinder contents. With the drop in temperatures during fuel injection after TDC, the rate of formation of soot is most likely decreasing. Furthermore, the amount of air entrainment before the standing premixed flame seems play a role in the overall soot formation process. Flynn et al showed [25] that as more oxygen is mixed with the fuel-rich vapor feeding the premixed flame, less carbon went into soot precursor formation and more went into forming carbon monoxide. Air entrainment increases as the unburned gases in the cylinder cool. Therefore, as timing is retarded away from TDC, the PM levels should drop as the data show since less soot is initially formed.

The high load particulate matter results are shown in Figure 27, which also shows the reduction of particulate matter switching to FT fuel from No. 2 diesel. The peak in-cylinder pressures and temperatures rise as load increases. With stock and reduced EGR rates, the oxidation mechanism seems to be dominant as timing is advanced due to the elevated bulk cylinder temperatures while reductions in soot oxidation as timing is retarded is accompanied by similar reductions in soot formation helping keep the overall PM output low. In the increased-EGR conditions, the rate of soot oxidation seems to be lower than its formation rate. The relatively smaller amount of fuel-air mixing may be contributing to this trend. As timing is retarded and air entrainment increases, the PM output level drops, suggesting the increased mixing reduces the soot formation rate.

Figure 27 Brake-specific particulate matter (bsPM) emissions versus the start of main injection timing for all experimental conditions at low loads. Solid lines apply to No. 2 diesel fuel and dashed lines apply to FT fuel. The individual data labels report the EGR rates for each condition. Enlarged data points represent stock timing condition.

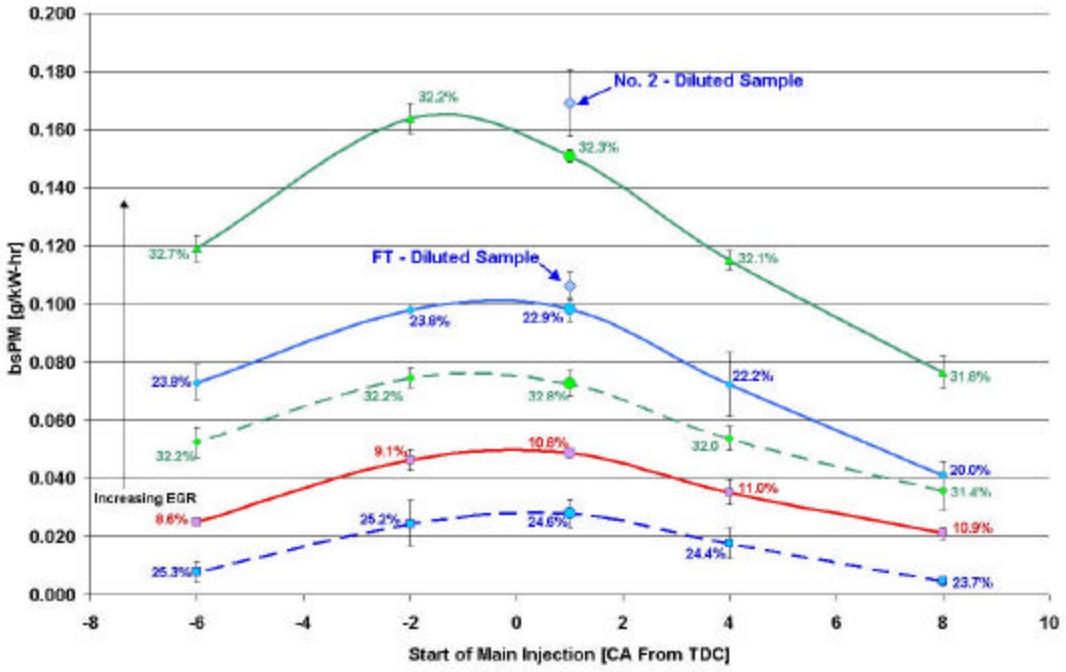

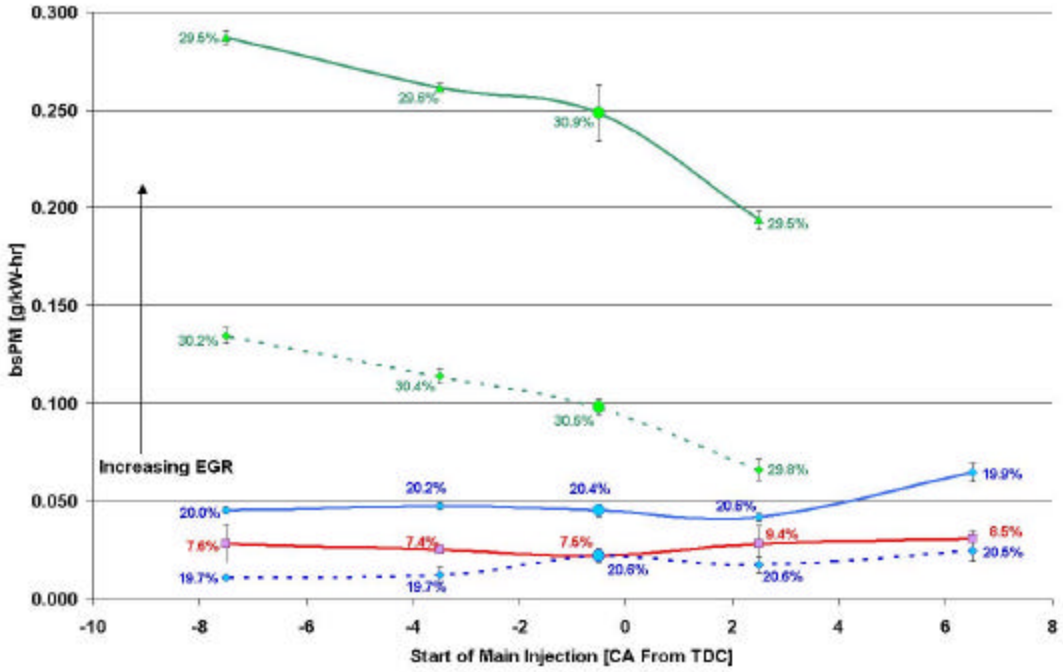

Figure 28 Brake-specific particulate matter (bsPM) emissions versus the start of main injection timing for all experimental conditions at high loads. Solid lines apply to No. 2 diesel fuel and dashed lines apply to FT fuel. The individual data labels report the EGR rates for each condition. Enlarged data points represent stock timing condition.

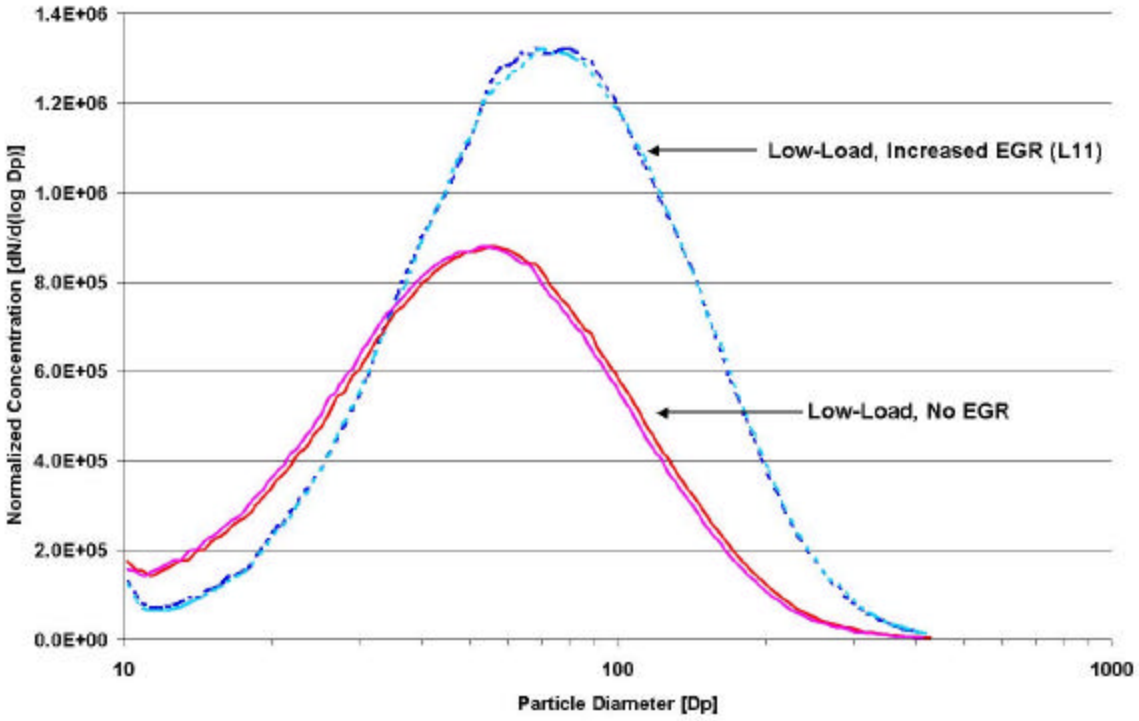

Figure 29 SMPS scans at low-load conditions with no EGR and increased-EGR settings.

Another trend common to both fuels shown in the aforementioned brake specific particulate matter results is the increase of PM as EGR rates increase. In general, EGR reduces the overall flame temperature through the increase in heat capacity of the recycled exhaust gases and reduces the oxygen concentration of the fresh air by diluting it with burned-gas products. The combination of the reduced temperature and oxygen concentration lowers the soot oxidation rate. A scanning-mobility particle size (SMPS) scan (see Figure 8.24) corroborates this by showing the size distribution moves towards more and larger particles. Since oxidation is less important, the soot formed initially can grow into larger carbonaceous agglomerates as combustion progresses.

Particulate Matter Emission Trends with Fuel Properties

Figures 8.26 and 8.27 show the low load and high load, respectively, of the brake specific NOx and PM for all the operating conditions for the two fuels. The FT fuel shows PM reductions in all operating conditions, consistent with many other results from the literature. The reductions ranged from about 53% – 56% at low loads and about 72% – 89% at high loads. Based on the raw sampling method, the PM collected in the experiments is most likely carbonaceous agglomerates. Therefore, the PM reductions must be related to the soot particles themselves, and not to the species that usually contribute to surface growth such as volatile species and sulfates. The reason for the

reduction in soot particles due to fuel properties is most likely the chemical structure of the fuels themselves.

Frenklach and Wang [30] and Richter et al [31] suggest that the initial inception of the smaller polycyclic aromatic hydrocarbons (PAHs) that eventually combine to form soot is dependent upon the availability of aromatic molecules after the initial breakdown of the fuel molecules. If aromatic molecules are present, the hydrogen-abstraction carbon-addition (HACA) mechanism can proceed directly on a simple aromatic to form the second aromatic rings. If, however, no aromatic molecules are present, acetylene must react to form the first ring, such that the above HACA mechanism can act upon this first ring to grow larger and larger particles. Therefore, based on the fact that the FT fuel from the Syntroleum Corporation has less than 0.001% by weight aromatics (see fuel specifications), more time is spent forming the first rings than growing larger PAHs, leading to a reduction in PM when using FT fuel.

Sulfate Contributions

The sulfur content obviously a major source of the reduction in the total particulate emissions measured when switching to the FT fuel. According to Kittelson et al [32], typical diesel exhaust (without any after-treatment devices) has sulfuric acid concentrations ranging from 5 – 20 PPM when using fuel with a sulfur content of 0.04% by mass. The No. 2 diesel used in the experiments has exactly this sulfur content, so estimations were made as to the sulfate contribution to PM for this fuel. Using this sulfate-exhaust concentration, the exhaust of the test engine should have sulfate levels between 0.015 – 0.060 g/kW-hr at the stock timing, stock EGR, low load condition, which accounts for a substantial fraction of the difference in particulate emission between the two fuels, as shown in Figure 8.26.

Conclusion

The Syntroleum plant is mechanically complete and currently undergoing start-up. The fuel production and demonstration plan is near completion. The study on the impact of SFP fuel on engine performance is about half-completed. Cold start testing has been completed. Preparations have been completed for testing the fuel in diesel electric generators in Alaska. Preparations are in progress for testing the fuel in bus fleets at Denali National Park and the Washington Metropolitan Transit Authority.

The experiments and analyses conducted during this project show that Fischer-Tropsch gas-to-liquid diesel fuel can easily be used in a diesel engine with little to no modifications. Additionally, based on the results and discussion presented, further improvements in performance and emissions can be realized by configuring the engine to take advantage of FT diesel fuel's properties. The FT fuel also shows excellent cold start properties and enabled the engine tested to start at more the ten degrees than traditional fuels would allow.

This plant produced through this project will produce large amounts of Fischer-Tropsch fuel. This will allow the fuel to be tested extensively, in current, prototype, and advanced diesel engines. The fuel may also contribute to the nation's energy security. The military has expressed interest in testing the fuel in aircraft and ground vehicles.

References

1. Alleman, T. L. and McCormick, R. L., "Fischer-Tropsch Diesel Fuels – Properties and Exhaust Emissions: A Literature Review," SAE Paper 2003-01-0763, 2003
2. Schaberg, P. W., Myburgh, I. S., Botha, J. J., Roets, P. N., Viljoen, C. L., Dancuart, L. P., and Starr M.E., "Diesel Exhaust Emissions Using Sasol Slurry Phase Distillate Process Fuels," SAE Paper 972898, 1997
3. Norton, P., Vertin, K., Bailey, B., Clark, N. N., Lyons, D. W., Goguen, S., and Eberhardt, J., "Emissions from Trucks using Fischer-Tropsch Diesel Fuel," SAE Paper 982526, 1998
4. Clark, N. N., Atkinson, C. M., Thompson, G. J. and Nine, R. D., "Transient Emissions Comparisons of Alternative Compression Ignition Fuels," SAE Paper 1999-01-1117, 1999
5. Atkinson, C. M., Thompson, G. J., Traver, M. L., and Clark, N. N., "In-Cylinder Combustion Pressure Characteristics of Fischer-Tropsch and Conventional Diesel Fuels in a Heavy Duty CI Engine," SAE Paper 1999-01-1472, 1999Fischer-Tropsch Website, http://www.fischer-tropsch.org/
4. Springer, P. S., Hugman, R. H., Costiness, M. J., Vidas, E. H., "Chemical Composition of Discovered and Undiscovered Natural Gas in the Continental United States – 1998 Update. Project Summary," Gas Research Institute, 1998
5. McMillian, M. H. and Gautam, M., "Consideration for Fischer-Tropsch Derived Liquid Fuels as a Fuel Injection Emission Control Parameter," SAE Paper 982489, 1998
6. Cheng, A. S. and Dibble, R. W., "Emissions Performance of Oxygenate-in-Diesel Blends and Fischer-Tropsch Diesel in a Compression Ignition Engine," SAE Paper 1999-01-3606, 1999
7. Schaberg, P. W., Myburgh, I. S., Botha, J. J. and Khalek, I. A., "Comparitive Emissions Performance of Sasol Fischer-Tropsch Diesel Fuel in Current and Older Technology Heavy-Duty Engines," SAE Paper 2000-01-1912, 2000
8. May, M. P., Vertin, K., Ren, S., Gui, X., Myburgh, I. And Schaberg, P., "Development of Truck Engine Technologies for Use with Fischer-Tropsch Fuels," SAE Paper 2001-01-3520, 2000
9. Suppes, G.J., Burkhart, M.L., Cordova, J.C., Sorem, R.M., Russell, B., "Performance of Fischer-Tropsch Liquids with Oxygenates in a VW 1.9L TDI" SAE Paper 2001-01-3521
10. Fanick, E.R., Schubert, P.F., Russell, B.J., Freerks, R.L., "Comparison of Emission Characteristics of Conventional, Hydrotreated, and Fischer-Tropsch Diesel Fuels in a Heavy-Duty Diesel Engine," SAE Paper 2001-01-3519
11. Nord, K. and Haupt, D., "Evaluating a Fischer-Tropsch Fuel, Eco-Par™, in a Valmet Diesel Engine," SAE Paper 2002-01-2726, 2002
12. EPA Test Procedure TP 713D, "Sample Collection, Continuous Hydrocarbon Analysis and Particulate Collection of the Light Duty Diesel Test Procedure"

13. EPA Test Procedure TP 714C, "Diesel Particulate Filter Handling and Weighing Procedure"
14. Hallgren, B. E., "Effects of Oxygenated Fuels on DI Diesel Combustion and Emission," M.S. Thesis, MIT, 20002
15. "Syntroleum S-2 Synthetic Diesel: Driving Clean-Fuel Innovation," http://www.syntroleum.com/media/syntroleum_s2.pdf, Syntroleum Corporation, 2002
16. Heywood, J. B., Internal Combustion Engine Fundamentals, McGraw-Hill, Inc., New York, 1988
17. DieselNet Website, http://www.dieselnet.com/
18. Payri, F., Arrègle, J., Fenollosa, C., Belot. G., Delage, A., Schaberg, P., Mybrugh, I., and Botha, J., "Characterization of the Injection-Combustion Process in a Common Rail D.I. Diesel Engine Running with Sasol Fischer-Tropsch Fuel," SAE Paper 2000-01-1803, 2001
19. Assanis, D. N., "A Computer Simulation of the Turbocharged Turbocompounded Diesel Engine System for Studies of Low Heat Rejection Engine Performance," Ph.D. Thesis, MIT, 1985
20. Dec, J. E., Espey, C., "Ignition and Early Soot Formation in a DI Diesel Engine Using Multiple 2-D Imaging Diagnostics," SAE Paper 950456, 1995
21. Dec, J. E., Coy, E. B., "OH Radical Imaging in a DI Diesel Engine and the Structure of the Early Diffusion Flame," SAE Paper 960831, 1996
22. Dec, J. E., "A Conceptual Model of DI Diesel Combustion Based on Laser-Sheet Imaging," SAE Paper 970873, 1997
23. Dec, J. E., Canaan, R. E., "PLIF Imaging of NO Formation in a DI Diesel Engine," SAE Paper 980147, 1998
24. Dec, J. E., Espey, C., "Chemiluminescence Imaging of Autoignition in a DI Diesel Engine," SAE Paper 982685, 1998
25. Flynn, P. F., Durrett, R. P., Hunter, G. L., zur Loye, A. O., Akinyemi, O. C., Dec, J. E., and Westbrook, C. K., "Diesel Combustion: An Integrated View Combining Laser Diagnostics, Chemical Kinetics, And Empirical Validation," SAE Paper 1999-01-0509, 1999
26. Siebers, D. and Higgins, B., "Flame Lift-Off on Direct-Injection Diesel Sprays Under Quiescent Conditions," SAE Paper 2001-01-0530, 2001
27. Naber, J. D. and Siebers, D., "Effects of Gas Density and Vaporization on Penetration and Dispersion of Diesel Sprays," SAE Paper 960034, 1996
28. Lee, R., Pedley, J., Hobbs, C., "Fuel Quality Impact on Heavy Duty Diesel Emissions: - A Literature Review," SAE Paper 982649, 1998
29. Kennedy, I. M., "Models of Soot Formation and Oxidation," Progress in Energy and Combustion Science, Vol. 23, Elsevier Science, 1997
30. Frenklach, M. and Wang, .H, "Detailed Modeling of Soot Particle Nucleation and Growth," Twenty-Third Symposium (International) on Combustion, The Combustion Institute, Pittsburgh, 1990

31. Richter, H., Grieco, W., and Howard, J., “Formation Mechanisms of Polycyclic Aromatic Hydrocarbons and Fullerenes in Premixed Benzene Flames,” Combustion and Flame, The Combustion Institute, 1999
32. Kittelson, D. B., Arnold, M. and Watts, and W. F. Jr., “Review of Diesel Particulate Matter Sampling Methods: Final Report,” University Of Minnesota, 1999
33. “Statement of Project Objectives,” Attachment A to Cooperative Agreement DE-FC26-01NT41099, July 20, 2001.